Precambrian Research 242 (2014) 138–153

Contents lists available at ScienceDirect

Precambrian Research

journal homepage: www.elsevier.com/locate/precamres

"Grenvillian" intra-plate mafic magmatism in the southwestern Yangtze Block, SW China

Wei Terry Chen[a], Wei-Hua Sun[b,*], Wei Wang[a], Jun-Hong Zhao[c], Mei-Fu Zhou[a]

[a] Department of Earth Sciences, University of Hong Kong, Pokfulam Road, Hong Kong, China
[b] School of Earth Sciences and Resources, China University of Geosciences, Beijing 100083, China
[c] State Key Laboratory of Geological Processes and Mineral Resources, China University of Geosciences, Wuhan 430074, China

ARTICLE INFO

Article history:
Received 24 September 2013
Received in revised form
23 December 2013
Accepted 30 December 2013
Available online 6 January 2014

Keywords:
Grenvillian
Julin Group
Passive continental margin
Yangtze Block
Rodinia

ABSTRACT

Tectonic affinity of Grenvillian magmatism in the South China Block is important for understanding the role of the block in the reconstruction of the Rodinia supercontinent during the Mesoproterozoic. In the southwestern Yangtze Block, South China, late Mesoproterozoic metabasalts occur as layers in the Pudeng Formation of the Julin Group. Most metabasalts are highly metamorphosed to be amphibolites composed of dominantly plagioclase and amphibole with minor Fe–Ti oxides, titanite and apatite. Two metabasalt samples have identical zircon U–Pb ages of ~1050 Ma. These basalts are tholeiitic in compositions and have high and variable TiO_2 (1.1–3.2 wt.%) and low Mg# values (=Mg/(Mg + Fe^{2+}); 35–60). In the primitive mantle-normalized diagram, they are characterized by enrichments in Th, Nb, Ta and light REE without significant Zr–Hf–Nb–Ta–Ti anomalies. The samples have $\varepsilon Nd(t)$ values ranging from −1.4 to +4.0 and their zircon grains have $\varepsilon Hf(t)$ values from −1.7 to +11.0. The low Mg# values and Cr (55.1–261 ppm) and Ni (13.5–76.5 ppm) contents suggest fractional crystallization of olivine and/or clinopyroxene, whereas minor negative Eu anomalies indicates slightly fractional crystallization of plagioclase. High positive $\varepsilon Nd(t)$ and $\varepsilon Hf(t)$ values suggest derivation of the parental magma from a depleted asthenospheric mantle source. On the other hand, variable $\varepsilon Nd(t)$ and $\varepsilon Hf(t)$ values and La/Sm and Nb/La ratios are consistent with significant crustal assimilation by the Paleoproterozoic rocks in the region. These samples have high Ti and Ti/V ratios (mostly >40), typical of within-plate basalts. In the Zr–Nb–Y and Th–Ta–Hf diagrams for tectonic discrimination, the samples with least crustal contamination are plotted in the 'within-plate' and 'E-MORB' fields, indicating an intra-continental rifting setting. In view of subsequent Neoproterozoic arc magmatic activities (950–730 Ma) in the region, we suggest that these basalts were likely produced at a rifting basin in a passive margin. Results presented here demonstrate that the Grenville-age magmatism in the southwestern Yangtze Block was not orogenic in origin, thus arguing against the existence of Grenvillian Orogen in the region that was traditionally used to place the South China Block in the central part of the Rodinia supercontinent.

1. Introduction

Worldwide Grenvillian orogenic events in the time period of ca. 1300–900 Ma were commonly associated with continental collisions during the assembly of the Neoproterozoic supercontinent Rodinia (e.g., Hoffman, 1991; Clarke et al., 1995; Burrett and Berry, 2000; Karlstrom et al., 2001; Boger et al., 2001; Jacobs et al., 2003). In South China, widespread deformation, regional unconformities and Proterozoic magmatism in the Jiangnan Fold Belt have long been thought to mark the Grenvillian orogenesis, forming the so-called Sibao Orogenic Belt that has been positioned in central Rodinia (Fig. 1) (e.g. Li et al., 1999, 2007, 2008, 2009; Greentree et al., 2006; Ye et al., 2007; Zhang et al., 2007; Yang et al., 2009). This orogenic belt was thought to extend from the southeast to the southwest margin of the Yangtze Block, and was produced by the amalgamation of the Yangtze Block and the Cathaysia Block (Fig. 1) (Li et al., 2002a). Widespread Neoproterozoic (850–740 Ma) magmatism has been interpreted to be related to the breakup of the Rodinia supercontinent (Li et al., 2002b). However, new geochronological and geochemical data of sedimentary rocks from the Jiangnan Fold Belt in the southeastern Yangtze Block indicates that this orogenic belt likely formed at Neoproterozoic (~830–815 Ma) rather than Mesoproterozoic as previously thought, and therefore the Yangtze Block cannot be affiliated with the Rodinia (Wang et al., 2010, 2012a,b, 2013; Wang and Zhou, 2012; Zhao et al., 2011), and that the Grenvillian orogen does not exist in the east (Zhao et al., 2011; Li et al., 2013). It is important to understand whether or not the Grenvillian orogenic magmatism

* Corresponding author. Tel.: +86 132 4165 2990.
E-mail address: weihuasun@yahoo.com (W.-H. Sun).

0301-9268/$ – see front matter © 2014 Elsevier B.V. All rights reserved.
http://dx.doi.org/10.1016/j.precamres.2013.12.019

occurred in the southwestern Yangtze Block that was considered to be part of the so-called Sibao Orogen.

In the southwestern Yangtze Block, late Meso- to early Neoproterozoic sedimentary strata are widespread, as best represented by the Kunyang, Huili and Julin Groups in different areas (Wu et al., 1990; Deng, 2000; Sun et al., 2009). Mesoproterozoic mafic and felsic volcanic rocks occur as interlayers in these sedimentary strata (Deng, 2000; Greentree et al., 2006; Geng et al., 2007; Zhang et al., 2007). The tectonic affinity of these volcanic rocks is key to understand the tectonic setting of the western Yangtze Block and thus the role of the Yangtze Block in Rodinia during the Mesoproterozoic. Nevertheless, precise age data of these igneous rocks is not available in literature. Likewise, their petrogenesis is poorly understood. Because mafic volcanic rocks (e.g., basalts) are derived from mantle sources directly, their compositions are widely used to constrain the nature of mantle sources and tectonic settings of the magmatic activities (Pearce and Cann, 1973). Thus, Mesoproterozoic basalts in the southwestern Yangtze Block provide a valuable opportunity to unravel the tectonic evolution of the southwestern Yangtze Block during the time period when these basalts erupted.

In this paper, we present new geochronological and geochemical data for the Mesoproterozoic metabasalts from the Julin Group in the southwestern Yangtze Block. These data provide tight constraints on the age, petrogenesis and tectonic setting of the basaltic magmatism. With these new results, the late Mesoproterozoic tectonic evolution of the southwestern Yangtze Block is discussed in the context of the Rodinia supercontinent assembly.

2. Geological background

2.1. Regional geology

The South China Craton consists of the Yangtze Block in the northwest and the Cathaysia Block in the southeast. The Yangtze Block is bounded by the Songpan-Ganze Terrane of the Tibetan Plateau to the west and is separated from the North China Craton by the Qinlin-Dabie-Sulu Orogen to the north (Fig. 1). The Precambrian lithology of the Yangtze Block is dominated by widespread Neoproterozoic igneous and sedimentary rocks (860–740 Ma) with sporadical exposure of Archean units, as best represented by the ~2.9–3.3 Ga Kongling tonalitic-trondhjemitic-granodioritic gneisses complex in the northern Yangtze Block (Qiu et al., 2000; Gao et al., 2011). The Kongling Complex was intruded by the ~1.85 Ga A-type granitic plutons and mafic dykes in the north (Peng et al., 2009; Xiong et al., 2009; Zhang et al., 2011) and the ~850 Ma Huangling tonalite-trondhjemite-granite complex in the south (Zhao et al., 2013a,b).

The southeastern and southwestern parts of the Yangtze Block are different in terms of Proterozoic strata in the Jiangnan Fold Belt. In the southeastern Yangtze Block, the early Neoproterozoic sedimentary strata are widely distributed (Gao et al., 2008; Zhao et al., 2011; Wang et al., 2010, 2012a,b, 2013), including the Sibao, Lengjiaxi, Fanjingshan, Shuangqiaoshan and Xikou Groups, which are intruded by numerous felsic and mafic plutons (Li et al., 2003; Zhao et al., 2013c). The late Neoproterozoic sedimentary strata, including the Danzhou, Banxi, Heshangzheng and Likou Groups, have deposited in the Nanhua rift basin and are unconformably overlain by the early Neoproterozoic strata (Wang and Li, 2003; Wang and Zhou, 2012). The glacial-interglacial sedimentary sequences have been recognized in several localities of the Hunan, Guizhou and Guangxi provinces (Zhang et al., 2003).

In the southwest, late Paleoproterozoic to early Neoproterozoic strata are widespread (Fig. 1). The Paleoproterozoic strata include the Dahongshan, Dongchuan and Hekou Groups which are characterized by upper greenschist to lower amphibolite facies metamorphism (Li et al., 1988), and are intruded by Paleoproterozoic gabbroic plutons (Zhao et al., 2010; Guan et al., 2011; Zhao and Zhou, 2011). Both the Dahongshan and Hekou Groups comprise a sequence of meta-volcano-sedimentary rocks, whereas the Dongchuan Group is dominated by sedimentary rocks including sandstone, slate and dolostones (Zhao et al., 2010). These Paleoproterozoic strata contain tuffaceous layers with zircon U–Pb ages of ~1700 Ma (Hu et al., 1991; Greentree and Li, 2008; Zhao et al., 2010; Yang et al., 2012).

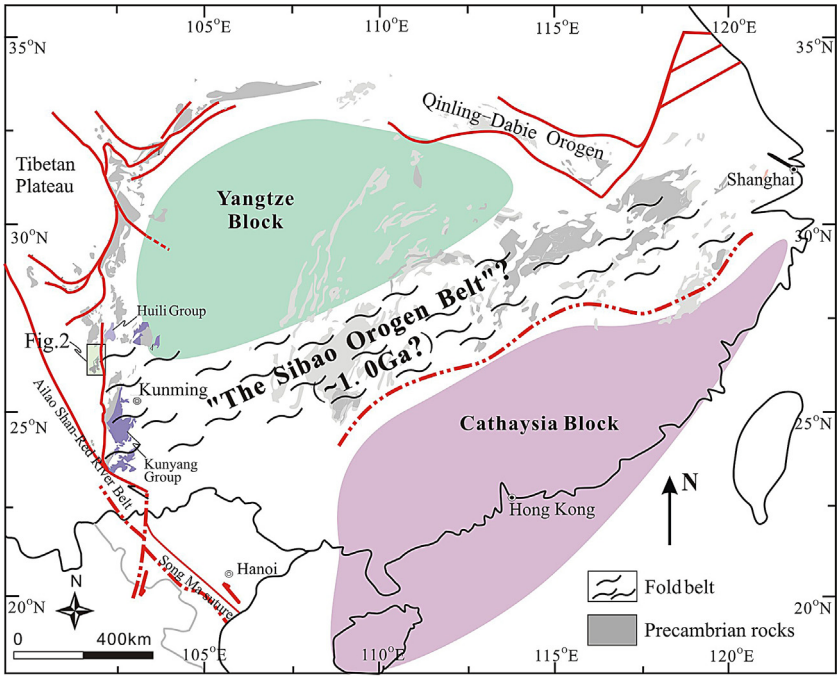

Fig. 1. Simplified tectonic framework of the South China Craton showing the distribution and timing of the traditionally proposed Mesoproterozoic Sibao orogen (modified after Li et al., 2002a).

Late Meso- to early Neo- Proterozoic strata in the southwestern Yangtze Block include the Kunyang, Huili, Julin and Yanbian groups (Fig. 1). Except with the Julin Group being locally metamorphosed to lower amphibolite facies (YBGMR, 1991; Deng, 2000), the other groups have underwent only lower greenschist facies metamorphism (Chen and Chen, 1987; Li et al., 1988). The Neoproterozoic Yanbian Group has detrital zircons as young as ~860 Ma (Zhou et al., 2006; Sun et al., 2009). The Meso- to Neo-Proterozoic strata in the region were emplaced by numerous Neoproterozoic igneous rocks including granites, diorites and gabbros in the time interval of ~860 to ~740 Ma (Zhou et al., 2002a,b, 2006; Li et al., 2003; Huang et al., 2008, 2009; Sun and Zhou, 2008; Zhao et al., 2008).

2.2. Julin Group and its equivalents

The Julin Group covers an area approximating 800 km^2 around the Yuanmou County in northern Yunnan Province (Fig. 2). It is intruded by numerous granitic and mafic-ultramafic plutons and doleritic and felsic dykes, such as the 746 Ma Yuanmou granitic complexes (Zhou et al., 2002b) and Permian Zhubu mafic-ultramafic pluton (Zhu et al., 2007). The Julin Group is in fault contact with the Jurassic to Cretaceous continental sediments to the east, and is unconformably overlain by Sinian and younger strata to the west and center (Fig. 2). The strata locally show strong schistosity and are tightly foliated with mineral lineation (e.g., Fig. 3a–c), but sedimentary structures such as cross-bedding are locally preserved in some meta-sandstones (YBGMR, 1991; Deng, 2000).

The Julin Group consists of the Pudeng, Lugumo, Fenghuangshan and Haizishao Formations from the base upward, and has a total thickness of >3560 m (Fig. 2) (cf. YBGMR, 1991). The Pudeng Formation consists dominantly of gneisses and schists with subordinate meta-volcanic rocks and marbles. The Lugumo Formation is dominated by massive quartzite and meta-sandstone with a thickness of 219–310 m. The Fenghuangshan Formation is mainly composed of marble and slightly deformed dolomite or limestone with minor interlayers of carbonaceous slate, phyllite and quartz schist. The Haizishao Formation is composed of sericite-chlorite phyllite, two micas and quartz schists with minor quartzite.

Equivalents to the Julin Group in this region are the Kunyang Group distributed in central and eastern Yunnan Province and the

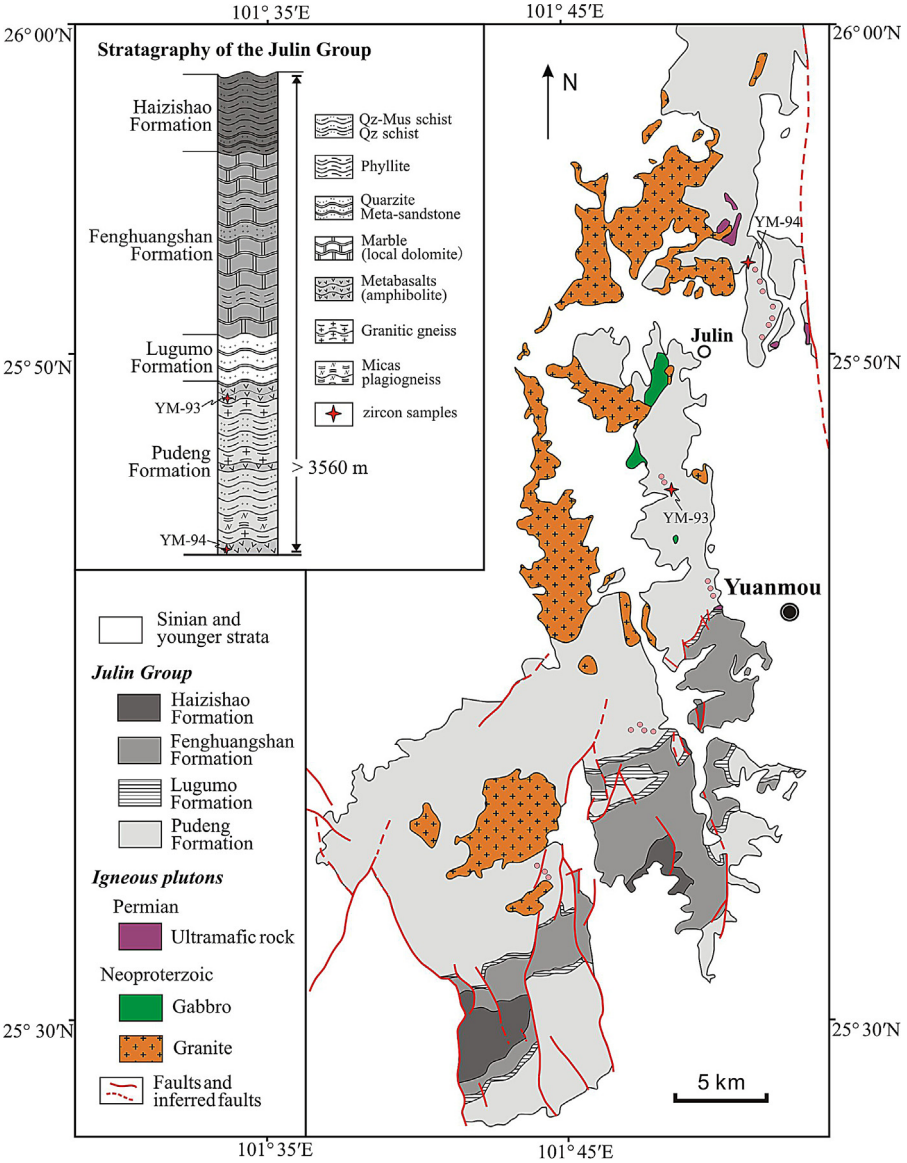

Fig. 2. A simplified geological map of the Yuanmou area (after YBGMR, 1991). Also shown is the stratagraphic column of the Julin Group. Locations of samples for zircon U–Pb dating are also shown.

Huili Group in southern Sichuan Province. The Kunyang Group is a flysch-like sequence consisting primarily of grey to dark carbonaceous slate, siltstone, sandstone and carbonate. It has been subdivided into the Dayingpan, Heishantou, Dalongkou, and Meidang Formations from the base upward (Wu et al., 1990; Zhao et al., 2010). Greentree et al. (2006) has identified the Laowushan Formation at the basal part of the Kunyang Group. There are minor intermediate volcanic layers occurring at uppermost unit of the Heishantou Formation and basaltic layers in the Laowushan Formation (e.g., Greentree et al., 2006). Zircon U–Pb dating of these volcanic layers constrained that the Kunyang Group have formed at ~960–1142 Ma (Greentree et al., 2006; Zhang et al., 2007).

The Huili Group, distributing in southernmost Sichuan Province, is a sequence of slate, siltstone, sandstone and carbonate, with felsic volcanic layers in its upper portion. It is divided into, from the base upward, the Tongan, Limahe, Fengshanying and Tianbaoshan Formations (BGMRSP, 1970). According to YBGMR (1991), the Pudeng Formation of the Julin Group is an equivalent of the Tongan Formation of the Huili Group, whereas the other three Formations are comparable to the Limahe, Fengshanying and Tianbaoshan Formations of the Huili Group. The Tianbaoshan Formation contains felsic volcanic layers with zircon U–Pb ages of ~1028 Ma (Geng et al., 2007; Sun et al., 2009).

3. Field relations and petrography of metabasalts

Abundant basaltic layers occur in the lower and upper parts of the Pudeng Formation of the Julin Group. These basaltic layers have a total thickness of >260 m. They are generally massive, and are locally interbedded with albitites, quartz schists and meta-tuff, some of which are primary felsic volcanic rocks in compositions (YBGMR, 1991) (Fig. 3c). Basaltic layers have also been documented in the Laowushan Formation, the basal unit of the Kunyang Group, which are interlayered with tuff dated at ca. 1142 Ma (Greentree et al., 2006).

These basaltic layers are amphibolites, and are mostly characterized by foliation due to mineral lineation (Fig. 3b). They are commonly massive, and are locally crosscut by quartz or carbonate veinlets. However, original volcanic structures such as porphyry and almonds are also preserved in some locations, and some phenocrysts are elongated plagioclase (YBGMR, 1991; Deng, 2000). They are dominantly composed of elongated amphibole and plagioclase (>80 vol.% in total) with subordinate titanite, Fe–Ti oxides and apatite (Fig. 3d), and thus were considered to be metamorphosed products of original basalts (YBGMR, 1991). There are also minor epidote, chlorite and quartz, as subsequent alteration products.

4. Analytical methods

4.1. LA-ICP-MS zircon U–Pb dating

Zircon grains were separated using magnetic and heavy liquid techniques, mounted in epoxy and polished to about half of their thicknesses. Cathodoluminescence imaging (CL) was used to investigate morphologies and internal structure of the crystals and

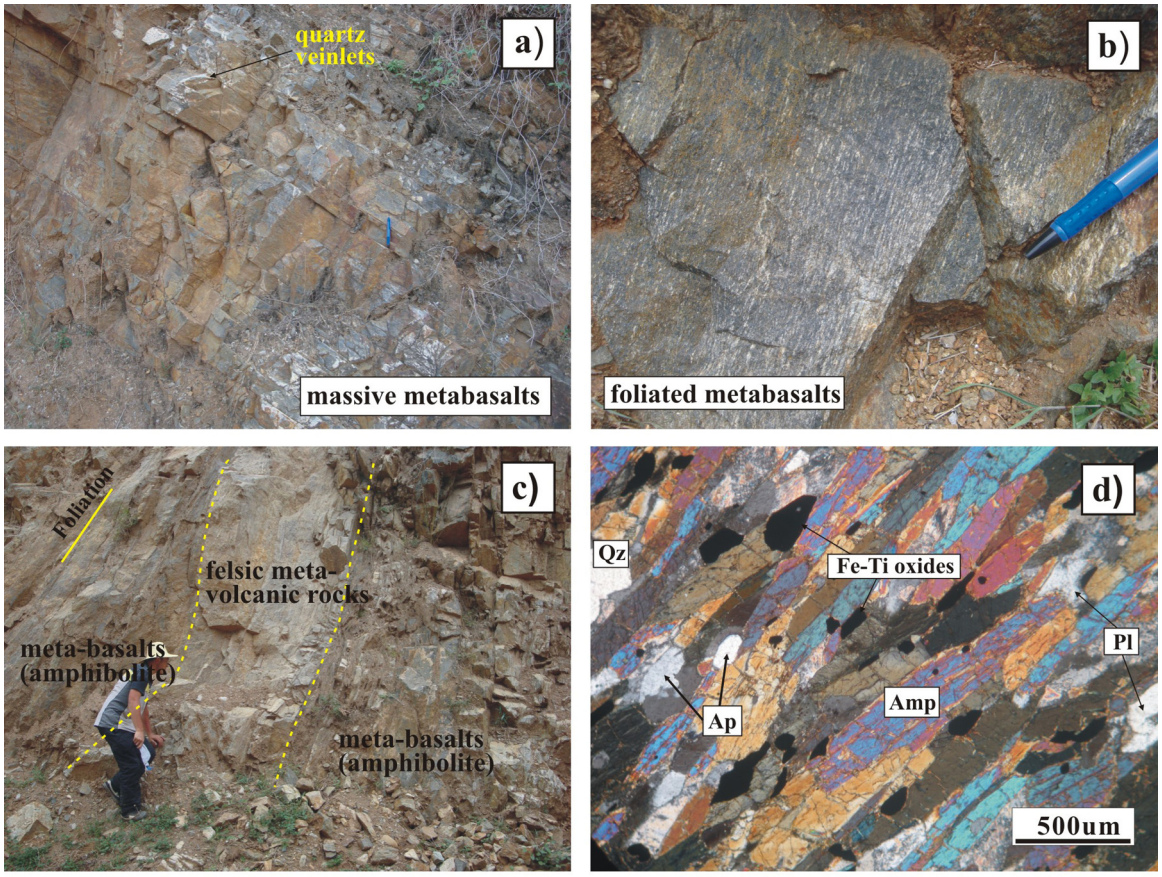

Fig. 3. Field and microscopic photos of the metabasalt layers in the Julin Group. (a) Massive metabasaltic layers which are crosscut by minor veinlets of carbonate or quartz; (b) foliated metabasalts characterized by lineation of plagioclase and amphibole; (c) metabasaltic layers are interlayered with felsic meta-volcanic rocks; (d) petromicrographic photos of foliated metabasalts (amphibolite). They are dominated by amphibole and plagioclase with subordinate Fe–Ti oxides, apatite, zircon and quartz. Mineral abbreviations: Pl – plagioclase; Amp – amphibole; Ap – apatite; Qz – quartz.

to select analytical spots. Uranium-lead isotopes of zircon grains were analyzed using the Nu Instrument multi-collector inductively coupled plasma-mass spectrometry (MC-ICP-MS), attached to the Resonetics RESOlution M-50-HR Excimer Laser Ablation System, at the University of Hong Kong. Analyses were performed with a beam diameter of 30 μm and 6 Hz repetition rate. Data acquisition started with a 30 s measurement of gas blank during the laser warm-up time. Typical ablation time was 40 s for each measurement, resulting in pits of 30–40 μm depth. ^{232}Th, ^{208}Pb, ^{207}Pb, ^{206}Pb, ^{204}Pb were simultaneously measured in static-collection mode. External corrections were applied to all unknowns, and standard zircons 91500 (^{206}Pb/^{238}U age = 1065.4 ± 0.6 Ma; Wiedenbeck et al., 1995) and GJ (^{206}Pb/^{238}U age = 599.8 ± 4.5 Ma; Jackson et al., 2004) were used as external standards and were analyzed twice before and after every 10 analyses. The raw data were reduced firstly by ICPMSDataCal program (Liu et al., 2008) and then were processed using the ISOPLOT program (Ludwig, 2003).

Table 1
LA-ICP-MS zircon U–Pb analyses of the metabasalts of the Julin Group.

Spot	Th (ppm)	U (ppm)	Th/U	^{207}Pb/^{206}Pb		^{207}Pb/^{235}U		^{206}Pb/^{238}U		^{207}Pb/^{206}Pb		^{207}Pb/^{235}U		^{206}Pb/^{238}U	
				Ratio	1σ	Ratio	1σ	Ratio	1σ	Age	1σ	Age	1σ	Age	1σ
YM-93 metabasalt															
1	142	611	0.23	0.0703	0.0004	1.5585	0.0118	0.1597	0.0009	936	13	954	5	955	5
2	562	520	1.07	0.0721	0.0006	1.7033	0.0143	0.1704	0.0008	987	17	1010	5	1014	4
3	1976	1142	1.70	0.0737	0.0008	1.6647	0.0169	0.1627	0.0009	1035	21	995	6	972	5
4	590	592	0.98	0.0712	0.0009	1.4706	0.0174	0.1487	0.0009	965	26	918	7	894	5
5	578	572	1.01	0.0729	0.0008	1.7283	0.0186	0.1712	0.0010	1011	24	1019	7	1019	5
6	2428	1031	2.33	0.0730	0.0008	1.3593	0.0154	0.1341	0.0009	1017	21	872	7	811	5
7	1419	1003	1.41	0.0727	0.0007	1.6440	0.0175	0.1629	0.0010	1006	20	987	7	973	6
8	527	668	0.78	0.0722	0.0008	1.6751	0.0192	0.1670	0.0009	991	23	999	7	995	5
9	201	299	0.67	0.0731	0.0011	1.7273	0.0242	0.1704	0.0012	1018	34	1019	9	1014	6
10	927	1204	0.78	0.0708	0.0009	1.6056	0.0213	0.1635	0.0011	950	26	972	8	976	6
11	510	454	1.11	0.0736	0.0010	1.7182	0.0218	0.1683	0.0010	1029	26	1015	8	1003	5
12	1072	759	1.41	0.0717	0.0009	1.6059	0.0190	0.1614	0.0010	977	29	973	7	965	5
13	2418	1757	1.37	0.0731	0.0007	1.7256	0.0174	0.1699	0.0009	1017	20	1018	6	1011	5
14	679	561	1.21	0.0739	0.0008	1.7241	0.0192	0.1682	0.0010	1039	22	1018	7	1002	6
15	496	406	1.22	0.0740	0.0009	1.6705	0.0205	0.1627	0.0011	1043	25	997	8	972	6
16	713	492	1.39	0.0741	0.0009	1.6953	0.0206	0.1648	0.0010	1044	56	1007	8	983	6
17	677	526	1.29	0.0742	0.0009	1.8223	0.0227	0.1771	0.0013	1047	19	1054	8	1051	7
18	874	939	0.94	0.0736	0.0008	1.7738	0.0210	0.1736	0.0013	1031	22	1036	8	1032	7
19	681	655	1.03	0.0745	0.0008	1.8217	0.0201	0.1762	0.0011	1057	21	1053	7	1046	6
20	828	915	0.90	0.0730	0.0007	1.5342	0.0163	0.1515	0.0009	1013	21	944	7	910	5
21	701	688	1.01	0.0747	0.0008	1.7090	0.0187	0.1649	0.0009	1061	22	1012	7	984	5
22	1246	885	1.37	0.0744	0.0009	1.7580	0.0202	0.1705	0.0010	1052	24	1030	7	1015	5
23	268	421	0.62	0.0740	0.0010	1.8060	0.0243	0.1764	0.0012	1043	28	1048	9	1047	6
24	874	1063	0.82	0.0727	0.0009	1.4359	0.0178	0.1423	0.0010	1007	24	904	7	858	6
25	759	818	0.92	0.0731	0.0008	1.7505	0.0222	0.1730	0.0016	1017	22	1027	8	1029	9
26	2467	1308	1.87	0.0733	0.0007	1.6131	0.0169	0.1587	0.0009	1021	16	975	7	949	5
27	1431	919	1.55	0.0729	0.0008	1.7008	0.0175	0.1677	0.0009	1013	21	1009	7	1000	5
28	1573	901	1.73	0.0734	0.0008	1.7095	0.0202	0.1678	0.0012	1025	18	1012	8	1000	7
29	281	296	0.95	0.0740	0.0011	1.8069	0.0262	0.1765	0.0013	1043	31	1048	9	1048	7
YM-94 metabasalt															
1	693	493	1.39	0.0735	0.0009	1.8044	0.0215	0.1769	0.0011	1028	24	1047	8	1050	6
2	601	457	1.27	0.0749	0.0009	1.8027	0.0222	0.1737	0.0012	1065	30	1046	8	1033	6
3	1338	821	1.60	0.0732	0.0008	1.7752	0.0197	0.1745	0.0010	1020	22	1036	7	1037	6
4	677	550	1.22	0.0736	0.0009	1.7368	0.0199	0.1700	0.0010	1031	24	1022	7	1012	5
5	361	451	0.80	0.0884	0.0010	2.0844	0.0238	0.1699	0.0010	1392	23	1144	8	1012	5
6	483	417	1.15	0.0741	0.0009	1.8157	0.0221	0.1764	0.0011	1044	56	1051	8	1047	6
7	919	705	1.29	0.0740	0.0009	1.8082	0.0208	0.1760	0.0010	1040	24	1048	8	1045	6
8	1635	876	1.81	0.0741	0.0009	1.6135	0.0202	0.1568	0.0011	1056	56	975	8	939	6
9	1583	1943	0.79	0.0726	0.0008	0.9442	0.0104	0.0937	0.0006	1011	18	675	5	578	4
10	905	781	1.15	0.0733	0.0008	1.7485	0.0197	0.1720	0.0011	1022	23	1027	7	1023	6
11	644	477	1.35	0.0742	0.0009	1.7640	0.0221	0.1713	0.0012	1048	20	1032	8	1019	7
12	1404	803	1.75	0.0717	0.0009	1.6803	0.0216	0.1690	0.0010	976	26	1001	8	1007	6
13	659	996	0.65	0.0705	0.0008	1.5480	0.0182	0.1581	0.0008	943	25	950	7	946	5
14	593	949	0.62	0.0726	0.0008	1.7423	0.0199	0.1727	0.0012	1003	18	1024	7	1027	7
15	464	798	0.58	0.0721	0.0009	1.6974	0.0205	0.1695	0.0010	991	25	1008	8	1009	6
16	635	592	1.03	0.0726	0.0008	1.7470	0.0202	0.1734	0.0010	1011	18	1026	7	1031	5
17	872	622	1.39	0.0726	0.0008	1.7414	0.0203	0.1727	0.0010	1011	18	1024	8	1027	5
18	3556	1094	3.16	0.0744	0.0008	1.8137	0.0196	0.1752	0.0010	1051	20	1050	7	1041	5
19	781	678	1.13	0.0747	0.0008	1.8225	0.0211	0.1754	0.0011	1061	22	1054	8	1042	6
20	1958	1225	1.58	0.0744	0.0009	1.7868	0.0196	0.1723	0.0010	1054	22	1041	7	1025	6
21	595	529	1.11	0.0743	0.0011	1.8054	0.0241	0.1748	0.0014	1050	30	1047	9	1039	8
22	1428	1171	1.22	0.0740	0.0009	1.8146	0.0214	0.1756	0.0012	1043	23	1051	8	1043	7
23	912	835	1.09	0.0745	0.0008	1.8022	0.0198	0.1735	0.0011	1054	22	1046	7	1032	6
24	546	930	0.59	0.0726	0.0010	1.7273	0.0242	0.1706	0.0013	1011	29	1019	9	1015	7
25	890	1436	0.62	0.0738	0.0008	1.4948	0.0160	0.1452	0.0009	1039	23	928	7	874	5
26	3067	2288	1.34	0.0735	0.0007	1.3630	0.0131	0.1327	0.0007	1029	20	873	6	803	4
27	1078	1272	0.85	0.0734	0.0008	1.6009	0.0186	0.1564	0.0011	1033	22	971	7	937	6
28	749	790	0.95	0.0744	0.0009	1.7082	0.0208	0.1646	0.0010	1054	24	1012	8	982	6
29	1074	1019	1.05	0.0776	0.0012	1.4386	0.0207	0.1331	0.0009	1144	30	905	9	806	5

No common lead is corrected.

4.2. Whole-rock major and trace elemental analyses

Samples were crushed and powered to 200 meshes in an agate mill. Major element abundances were obtained using X-ray fluorescence (XRF) on fused glass beads at the University of Hong Kong. The accuracies of the XRF analyses are estimated to be ±1% (relative) for SiO_2, ±2% (relative) for other oxides present in concentrations greater than 0.5 wt.% and ±5% (relative) for minor oxides present in concentrations greater than 0.1%.

Trace elements were analyzed using a Quadrupole ICP-MS at the State Key Laboratory of Ore Deposit Geochemistry, Institute of Geochemistry, Chinese Academy of Sciences, Guiyang. Closed beakers in high-pressure bombs were used to ensure complete digestion (Qi et al., 2000). This analytical procedure is particularly suitable for analyzing Zr and Hf because zircon grains are completely dissolved with a recovery of nearly 100%. Pure elemental standards for external calibration, and OU-1 and AMH-1 as reference materials were used. Detailed procedures are given in Qi et al. (2000). Analyses for trace elements have accuracies better than 5%.

4.3. Whole-rock Sm–Nd isotope analyses

Sample powders were dissolved in Teflon bombs with $HF + HNO_3$ acid, and separated by the conventional cation-exchange technique. Total procedural blanks were <60 pg for Nd. Nd isotopic compositions were determined using a Neptune Plus multicollector mass spectrometer at Guangzhou Institute of Geochemistry, Chinese Academy of Sciences. The mass fractionation correction for Nd isotopic ratios was based on $^{146}Nd/^{144}Nd = 0.7219$. The standard materials, JNdi-1 and BHVO-2, measured together with samples, have average $^{143}Nd/^{144}Nd$ ratios of 0.512085 ± 0.000006 (2σ) and 0.512962 ± 0.000004 (2σ), respectively, in agreement with recommended values (e.g., Chauvel et al., 2011). Detailed procedures for Nd isotope analyses are available in Li et al. (2004).

4.4. Zircon Lu–Hf isotope analyses

Spots on zircon grains from Sample YM-93, previously analyzed with for U–Pb isotopes, were selected for Hf isotope measurement with a Nu Plasma HR MC-ICP-MS (Nu Instruments, UK), coupled with a 193 nm excimer laser ablation system (RESOlution M-50, Resonetics LLC, USA), hosted in the Department of Earth Sciences, the University of Hong Kong. Analyses were carried out with beam diameter of 33 μm, repetition rate of 10 Hz and typical ablation times of 40 s, resulting in 30–40 μm deep pits. Atomic masses 172–179 were simultaneously measured in

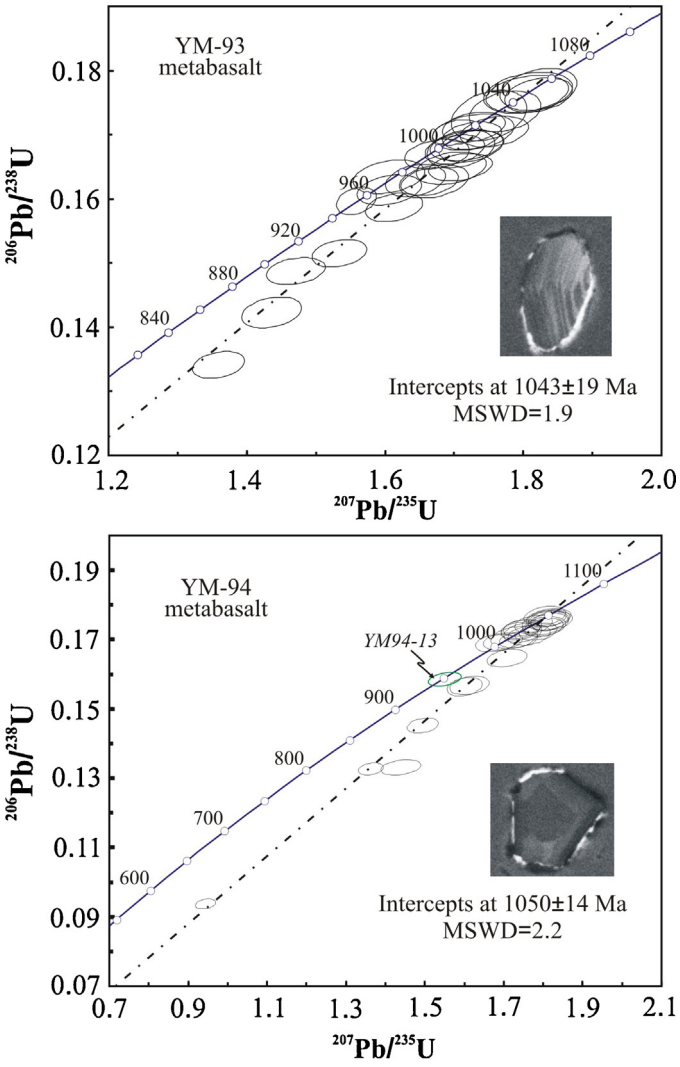

Fig. 4. U–Pb isotopic concordia plots of zircon grains from two metabasaltic samples of the Julin Group. Also shown are representative CL images.

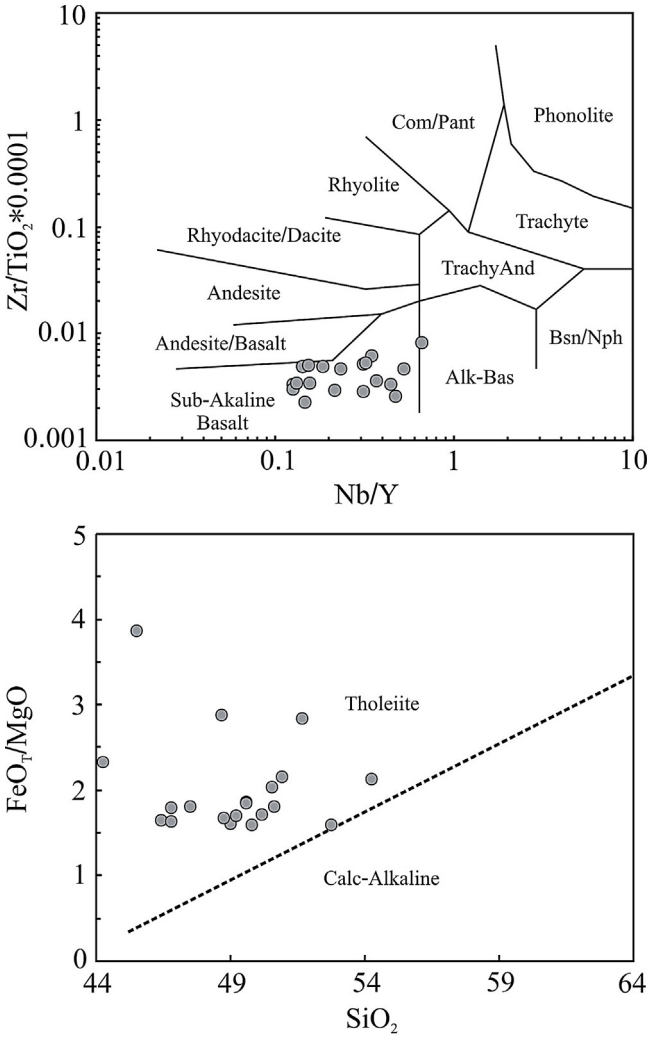

Fig. 5. Rock classification diagram of the metabasalts in the Julin Group. (a) The Nb/Y versus $Zr/TiO_2 \times 0.0001$ diagram distinguishing subalkaline and alkaline basalts (Winchester and Floyd, 1976, 1977); (b) FeO_T/MgO versus SiO_2 diagram distinguishing tholeiitic and calc-alkaline series (Miyashiro, 1974).

static-collection mode. Isobaric interference of ^{176}Yb on ^{176}Hf was corrected against the $^{176}Yb/^{172}Yb$ ratio of 0.5886 (Chu et al., 2002). Interference of ^{176}Lu on ^{176}Hf was corrected by measuring the intensity of the interference-free ^{175}Lu isotope and using a recommended $^{176}Lu/^{175}Lu$ ratio of 0.02655 (Machado and Simonetti, 2001). External calibration was made by measuring zircon standard 91500 and GJ-1 as unknowns. The measured $^{176}Lu/^{177}Hf$ ratios and a ^{176}Lu decay constant of 1.865×10^{-11} a^{-1} (Scherer et al., 2001) were used to calculate initial $^{176}Hf/^{177}Hf$ ratios. Calculation of $\varepsilon Hf(t)$ is based on the chondritic values of $^{176}Hf/^{177}Hf$ and $^{176}Lu/^{177}Hf$ reported by Blichert-Toft and Albarède (1997). Single-stage model ages (T_{DM1}) were calculated using the present-day ratios of $^{176}Hf/^{177}Hf$ (0.28325) and $^{176}Lu/^{177}Hf$ (0.0384) (Griffin et al., 2000). Two-stage model ages (T_{DM2}) were calculated by projecting the initial $^{176}Hf/^{177}Hf$ ratios of the zircon back to the depleted mantle model growth curve, assuming a $^{176}Lu/^{177}Hf$ value of 0.022 for the average continental crust (Amelin et al., 1999).

5. Results

5.1. Zircon U–Pb ages

Zircon grains of two metabasalts (YM-93 and YM-94) collected from the Pudeng Formation (Fig. 2) are analyzed. Zircon grains from these samples are mostly elongated with length <100 μm and show regular oscillatory zoning in the CL images (Fig. 4).

Twenty-nine zircon grains from sample YM-93 have 300–1700 ppm U and 200–2500 ppm Th with Th/U ratios ranging from 0.8 to 2.5 (Table 1), consistent with a magmatic origin. Most grains have concordant or marginally concordant U–Pb ages, but four grains (spots 4, 6, 20, and 24) are discordant (Fig. 4). The analyses yield an upper intercepted age of 1043 ± 19 Ma (MSWD = 1.9; Fig. 4).

Twenty-nine zircon grains from sample YM-94 have 500–1200 ppm U and 500–3000 ppm Th with Th/U ratios ranging from 0.6 to 1.4 (Table 1). Most spot analyses yield concordant U–Pb ages (Fig. 4). Spots 05 and 13 were excluded from age calculations as they have much older and younger apparent ages, respectively (Table 1). The remaining 27 analyses yield an upper intercepted age of 1050 ± 14 Ma (MSWD = 2.2; Fig. 4), identical to the value of sample YM-93 within uncertainty.

5.2. Major and trace elements

Most samples have high loss on ignition (L.O.I) up to 6.48 wt.%, presumably due to metamorphism and alteration (Table 2). In this case, major elements were normalized to 100 wt.% on a volatile free basis (Table 2). The metabasalts have wide ranges of major element abundances (SiO_2 = 44–55 wt.%; MgO = 3–10 wt.%; TiO_2 = 1.1–3.2 wt.%) (Table 2). In the Zr/TiO_2 versus Nb/Y plots (Winchester and Floyd, 1976), the samples have low Nb/Y

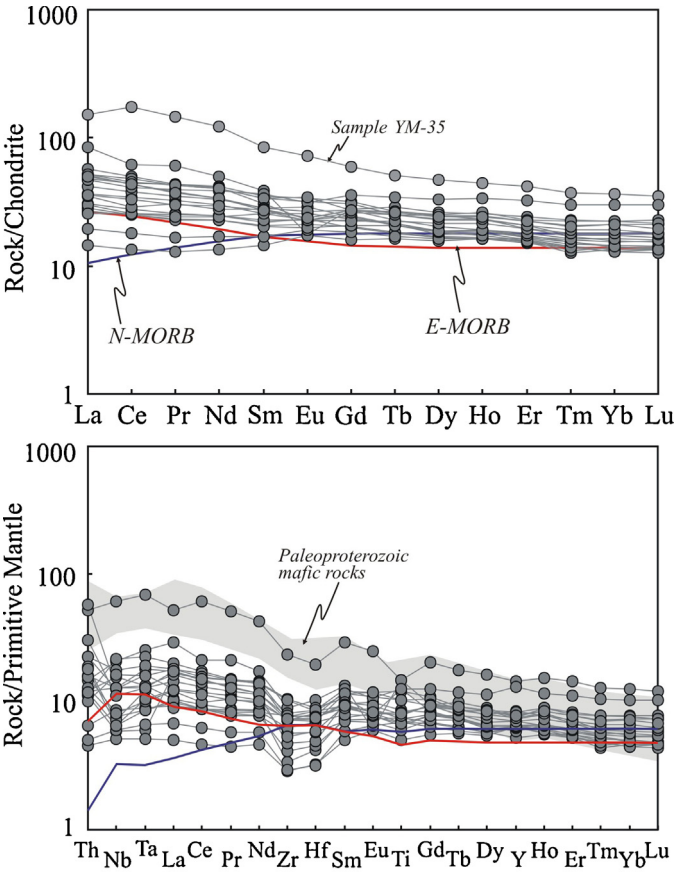

Fig. 6. Chondrite-normalized REE patterns and primitive-mantle normalized multi-elemental spider diagrams of the metabasalts in the Julin Group. Also plotted are those of N-MORB, E-MORB and Paleoproterozoic mafic rocks in the same region. Values of N-MORB, E-MORB, Chondrite and primitive mantle are after Sun and McDonough (1989), while those of the Paleoproterozoic mafic rocks are from Chen et al. (2013).

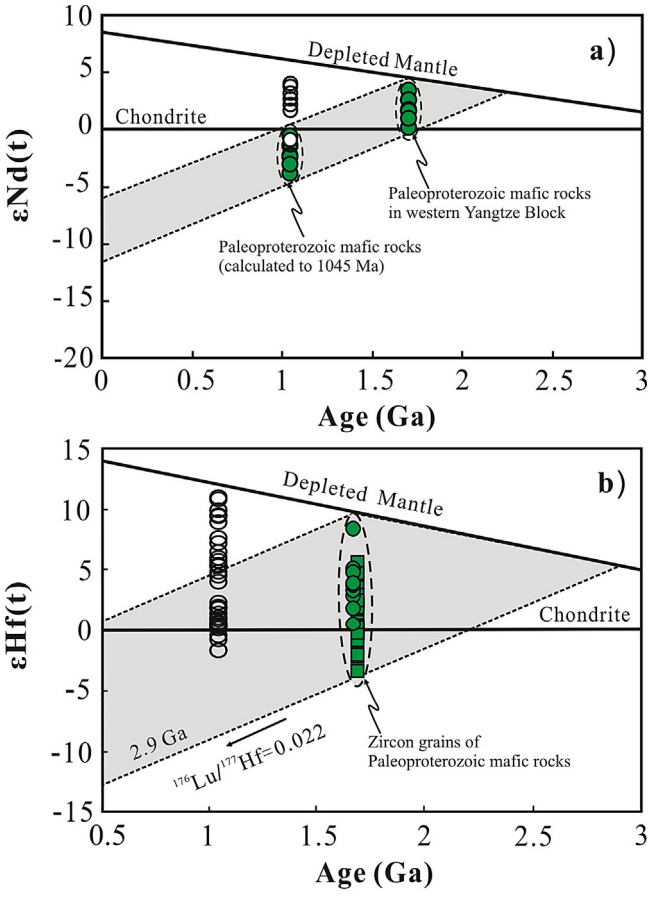

Fig. 7. (a) Plots of whole-rock $\varepsilon Nd(t)$ versus age for the metabasalts in the Julin Group. (b) Plots of $\varepsilon Hf(t)$ versus age for zircon grains from a metabasaltic sample (YM-93). Also plotted are whole-rock $\varepsilon Nd(t)$ and zircon $\varepsilon Hf(t)$ values of the Paleoproterozoic mafic rocks in the southwestern Yangtze Block (data from Zhao et al., 2010; Chen et al., 2013). The $\varepsilon Nd(t)$ and $\varepsilon Hf(t)$ values of the Paleoproterozoic mafic rocks were re-calculated to 1050 Ma for comparison.

Table 2
Major and trace elemental compositions of the metabasalts of the Julin Group.

Sample	YM35	YM55	YM92	YM93	YM94	YM107	YM202	YM203	YM206	YM208	YM209
SiO_2	54.24	49.02	49.20	49.79	52.74	50.92	48.74	50.17	44.26	49.58	47.51
TiO_2	3.22	3.22	1.61	1.50	1.42	2.61	1.62	1.10	2.72	2.22	1.49
Al_2O_3	13.39	17.84	14.76	14.42	14.65	13.51	15.03	14.65	17.83	15.86	15.59
Fe_2O_{3T}	10.87	16.02	12.80	12.26	11.08	15.75	13.48	13.40	20.22	13.53	14.72
MnO	0.14	0.04	0.21	0.20	0.18	0.24	0.22	0.22	0.26	0.27	0.23
MgO	4.65	9.36	7.04	7.18	6.55	6.67	7.50	7.27	7.85	6.69	7.53
CaO	6.88	0.76	9.49	9.38	7.61	7.90	9.79	9.60	2.79	8.46	9.75
Na_2O	5.55	3.10	2.26	2.64	3.30	1.25	2.03	1.62	0.83	1.81	1.65
K_2O	0.25	0.23	2.48	2.46	2.34	1.01	1.41	1.87	2.85	1.29	1.42
P_2O_5	0.81	0.41	0.15	0.16	0.14	0.15	0.17	0.09	0.37	0.29	0.12
Total	100.00	100.00	100.00	100.00	100.00	100.00	100.00	100.00	100.00	100.00	100.00
L.O.I	0.57	6.00	1.24	1.62	1.47	1.10	1.90	1.92	6.22	1.91	1.64
V	375	309	223	255	240	231	193	186	163	205	191
Cr	4.87	235	249	247	218	187	135	204	55.2	144	108
Co	32.1	23.3	48.5	38.1	36.0	36.3	1.8	41.3	44.6	39.8	55.1
Ni	43.2	62.8	63.3	59.1	53.5	47.8	56.9	32.4	71.6	88.7	74.2
Rb	7.51	15.0	145	161	152	42.1	69.5	105	150	64.7	50.5
Sr	84.5	60.9	201	165	135	132	180	186	119	130	118
Y	65.9	33.9	28.9	24.0	26.6	33.8	28.8	29.1	29.4	38.8	28.9
Zr	260	102	80.9	38.2	86.4	85.3	46.6	32.5	118	116	32.9
Nb	43.5	14.9	9.05	11.3	9.21	4.25	6.21	3.68	15.3	12.6	4.27
Cs	0.33	0.95	2.25	2.41	1.66	1.69	0.79	0.88	1.94	2.95	0.86
Ba	34.1	64.8	276	237	236	112	151	164	357	120	152
La	36.0	20.1	8.68	7.22	12.0	11.5	6.38	3.43	13.7	12.5	4.65
Ce	108	38.0	21.2	17.0	26.5	27.5	15.6	8.21	30.7	29.4	11.1
Pr	14.0	5.81	3.10	2.43	3.61	4.13	2.23	1.22	4.18	4.07	1.59
Nd	58.1	23.5	14.1	11.6	15.9	19.5	10.6	6.33	19.1	18.9	7.91
Sm	12.9	5.96	3.94	3.35	4.18	5.40	3.19	2.00	4.74	5.18	2.63
Eu	4.19	1.02	1.48	1.36	1.30	1.98	1.23	1.01	1.34	1.85	1.11
Gd	12.2	5.75	4.80	4.07	4.67	6.58	4.16	3.32	5.09	6.27	3.80
Tb	1.92	1.08	0.81	0.67	0.80	1.00	0.69	0.61	0.80	0.94	0.64
Dy	12.0	6.69	4.77	4.26	4.69	6.34	4.31	4.04	4.54	5.87	4.18
Ho	2.54	1.47	1.06	0.92	1.07	1.31	0.95	0.94	1.02	1.29	0.93
Er	6.96	4.02	2.81	2.51	2.76	3.25	2.54	2.69	2.68	3.43	2.63
Tm	0.95	0.58	0.41	0.36	0.40	0.44	0.33	0.38	0.37	0.45	0.34
Yb	6.24	3.82	2.61	2.20	2.41	2.67	2.28	2.49	2.30	2.94	2.38
Lu	0.90	0.58	0.40	0.34	0.35	0.39	0.35	0.36	0.34	0.43	0.36
Hf	6.03	3.20	2.51	1.31	2.59	2.43	1.40	1.00	2.76	2.60	0.98
Ta	2.82	1.04	0.67	0.55	0.74	0.25	0.37	0.21	0.93	0.78	0.28
Th	4.44	1.26	1.93	1.03	4.87	0.96	0.56	0.39	0.97	1.93	0.43
U	1.86	12.3	0.48	0.25	0.87	0.20	0.34	0.23	0.77	0.42	0.10

Sample	YM210	YM211	YM212	YM11-4	YM11-5	YM11-6	YM11-7	YM11-8	YM11-9	YM12-22
SiO_2	50.54	48.67	49.59	45.49	50.61	46.77	51.68	46.41	46.79	49.32
TiO_2	1.89	2.72	2.26	1.30	1.47	1.80	1.74	1.68	1.77	3.10
Al_2O_3	16.77	13.24	15.89	17.44	14.01	14.69	14.18	14.80	14.42	14.12
Fe_2O_{3T}	12.54	18.32	13.99	12.97	13.25	16.10	13.30	15.47	15.36	16.51
MnO	0.21	0.27	0.19	0.15	0.20	0.28	0.19	0.28	0.26	0.26
MgO	5.67	5.70	7.02	2.99	6.81	8.29	4.19	8.75	8.82	5.31
CaO	7.18	8.78	7.86	19.11	11.30	9.10	13.10	9.56	9.84	9.10
Na_2O	2.35	0.87	1.47	0.27	1.74	2.63	1.22	2.72	2.28	0.70
K_2O	2.64	1.20	1.43	0.06	0.47	0.22	0.17	0.23	0.39	1.18
P_2O_5	0.21	0.25	0.29	0.22	0.13	0.11	0.23	0.09	0.07	0.40
Total	100.00	100.00	100.00	100.00	100.00	100.00	100.00	100.00	100.00	100.00
L.O.I	1.82	1.58	1.19	0.99	1.16	0.98	0.80	0.87	1.01	1.25
V	203	146	193	342	251	255	256	275	263	308
Cr	122	137	115	131	261	183	163	163	226	137
Co	34.6	35.0	39.5	22.7	45.8	58.1	37.2	62.5	58.6	38.5
Ni	42.4	13.5	76.5	39.2	48.9	70.0	43.7	67.9	74.2	16.1
Rb	140	36.7	70.5	1.92	15.1	5.97	5.80	10.4	14.3	63.6
Sr	225	104	116	291	228	117	323	128	144	150
Y	29.9	59.3	31.9	29.9	32.4	36.1	34.0	37.7	35.5	45.5
Zr	53.3	91.7	80.7	63.2	70.6	87.6	80.5	82.4	59.6	120
Nb	9.25	9.20	11.7	5.49	4.64	5.12	7.95	5.83	4.70	18.0
Cs	1.02	0.62	1.86	0.06	0.35	0.15	0.13	0.12	0.26	2.12
Ba	300	182	154	19.6	154	60.5	52.1	64.4	151	123
La	10.0	11.2	12.3	6.79	7.10	6.16	11.9	8.33	8.52	20.3
Ce	23.2	25.3	28.0	15.6	15.6	15.6	26.8	17.7	20.3	39.1
Pr	3.37	3.78	4.06	2.16	2.38	2.30	3.55	2.90	2.87	5.62
Nd	15.4	18.0	18.9	10.7	11.6	11.3	15.9	13.1	13.7	25.1
Sm	4.31	5.60	5.20	3.14	3.54	3.97	4.37	4.27	4.14	6.83
Eu	1.67	1.80	1.99	1.17	1.32	1.34	1.57	1.39	1.39	2.22

Table 2
(*Continued*)

Sample	YM210	YM211	YM212	YM11-4	YM11-5	YM11-6	YM11-7	YM11-8	YM11-9	YM12-22
Gd	4.98	7.45	5.57	4.30	4.65	5.42	5.61	5.64	5.58	7.86
Tb	0.78	1.28	0.86	0.77	0.84	0.94	0.95	0.99	0.99	1.33
Dy	4.69	8.42	5.16	4.83	5.50	6.23	5.89	6.38	6.22	8.14
Ho	0.98	1.90	1.08	1.10	1.22	1.40	1.32	1.47	1.38	1.71
Er	2.59	5.37	2.88	2.97	3.26	3.73	3.42	3.80	3.72	4.79
Tm	0.36	0.77	0.39	0.42	0.46	0.53	0.49	0.57	0.52	0.69
Yb	2.22	5.07	2.42	2.78	3.08	3.63	3.28	3.78	3.58	4.29
Lu	0.32	0.77	0.34	0.41	0.45	0.54	0.46	0.55	0.50	0.63
Hf	1.54	2.69	2.18	1.78	2.15	2.36	2.29	2.32	1.81	3.18
Ta	0.53	0.55	0.66	0.35	0.36	0.51	0.53	0.42	0.43	1.03
Th	1.04	1.37	0.86	1.10	1.02	1.60	2.59	1.33	1.55	2.59
U	0.29	0.47	0.29	0.34	0.24	0.14	0.62	0.11	0.18	1.05

Fe_2O_{3T}: Fe_2O_3 total.

ratios of 0.10–0.66, falling in the sub-alkaline field (Fig. 5a). Moreover, all samples exhibit compositional trends typical of tholeiites in the FeO_T/MgO versus SiO_2 diagram (Fig. 5b). The rocks have a large range of Mg# values from 35 to 60 (Table 2). There is a narrow range of Al_2O_3 (13–18 wt.%) that do not show obvious correlation with Mg#. The CaO and P_2O_5 contents vary mostly from 1 to 15 wt.% and 0.1 to 0.5 wt.%, respectively, and both being roughly negatively correlated with Mg#.

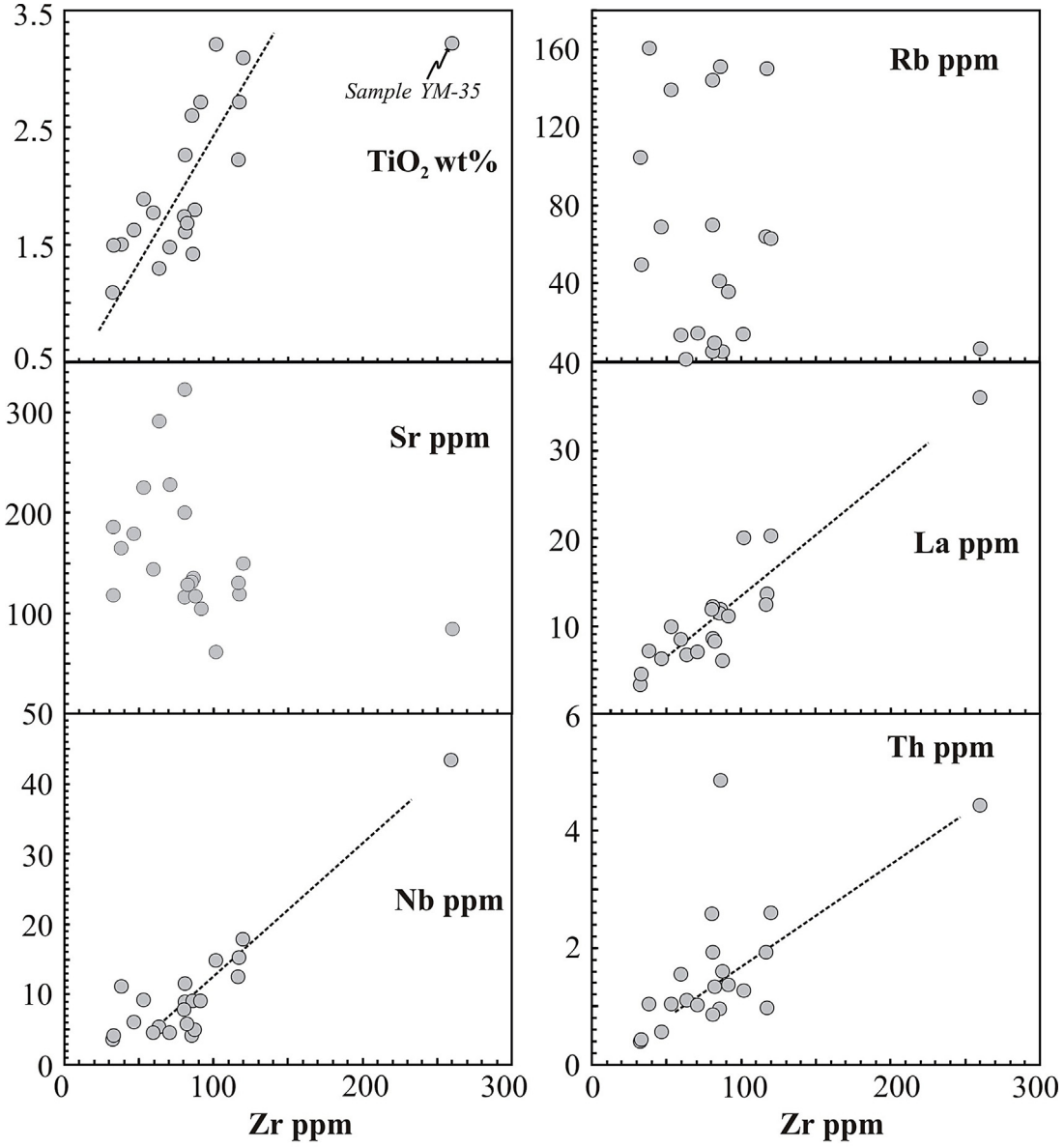

Fig. 8. Bi-elemental plots of TiO_2, Rb, Sr, La, Nb and Th versus Zr to evaluate the mobility of these elements of the metabasalts during metamorphism and hydrothermal alteration.

Table 3
Whole-rock Sm–Nd isotopic compositions of the metabasalts of the Julin Group.

Sample	Rock	Age (Ma)	Sm (ppm)	Nd (ppm)	$^{147}Sm/^{144}Nd$	$^{143}Nd/^{144}Nd$	$(^{143}Nd/^{144}Nd)_i$	$\varepsilon Nd(t)$	T_{DM} (Ma)
YM-55	Basalt	1050	5.96	23.5	0.153413	0.512265	0.511213	−1.4	2228
YM-202	Basalt	1050	3.19	10.6	0.181440	0.512614	0.511370	1.7	2520
YM-203	Basalt	1050	2.00	6.33	0.191090	0.512869	0.511559	5.4	1889
YM11-05	Basalt	1050	3.54	11.6	0.184664	0.512712	0.511446	3.2	2289
YM-3	Basalt	1050	3.76	13.4	0.169906	0.512652	0.511487	4.0	1729
YM-9	Basalt	1050	7.23	30.1	0.145252	0.512415	0.511419	2.7	1633

YM-3 and YM-9 are from Deng (2000).

The metabasalts have low Cr (55.2–261 ppm) and Ni (13.5–76.5 ppm) contents, which are negatively correlated with Zr (32.5–120 ppm). In addition, these samples have variable total REE contents (mostly 30–140 ppm) that is positively correlated with Zr. They have variable Th contents of 0.4–4.4 ppm, positively correlated with U (0.4–4.9 ppm), except for the sample YM-55 with the highest U (12.3 ppm) but lower Th (1.3 ppm) (Table 2).

The metabasalts are slightly enriched in LREE in the chondrite-normalized REE patterns (La/Yb_N = 1.0–4.2), which are roughly parallel to the Enriched Mid-Ocean Ridge Basalts (E-MORB) (Fig. 6). Most metabasalts do not show obvious Eu anomalies (Fig. 6). In the primitive-mantle normalized spider diagram, they have slightly negative Zr–Hf (Hf/Sm_{PM} = 0.5–0.9) and slightly positive to negative Nb–Ta anomalies (Ta/La_{PM} = 0.4–1.4) (Fig. 6). The sample YM-35 has relatively high LREE and HSFE with a slightly negative Ti anomaly (Fig. 6).

5.3. Whole-rock Sm–Nd and zircon Lu–Hf isotopes

The metabasalts have measured $^{143}Nd/^{144}Nd$ ratios ranging from 0.512265 to 0.512712. These values correspond to initial $^{143}Nd/^{144}Nd$ ratios of 0.511213 to 0.511446 and $\varepsilon Nd(t)$ values of −1.4 to +4.0 (Fig. 7a; Table 3).

Lu–Hf analyses were conducted on zircon grains from the sample YM-93, previously analyzed for U–Pb isotopes. The initial $\varepsilon Hf(t)$ values of zircons and their depleted mantle model ages (T_{DM1} and T_{DM2}) were calculated using their crystallization ages (1050 Ma). These zircon grains have variable $\varepsilon Hf(t)$ values from −1.7 to +11.0, slightly lower than that of the depleted mantle at 1050 Ma (Fig. 7b). They have single-stage Hf model ages ranging from 1135 to 1647 Ma (Table 4).

6. Discussion

6.1. Effects of metamorphism and alteration on elemental mobilities

The metabasalts from the Julin Group have undergone variable degrees of metamorphism and hydrothermal alterations, as indicated by the presence of amphibole and minor chlorite, quartz and epidote, as well as high L.O.I values (Table 2). Zirconium, one of the most immobile element during low-grade metamorphism and

Table 4
Zircon Lu–Hf isotopic compositions of the metabasalts of the Hekou Group.

Spot	Age (Ma)	$^{176}Yb/^{177}Hf$	$^{176}Lu/^{177}Hf$	$^{176}Hf/^{177}Hf$	1σ	Hf_i	$\varepsilon Hf(0)$	$\varepsilon Hf(t)$	T_{DM1} (Ma)	T_{DM2} (Ma)	$f_{Lu/Hf}$
1	1050	0.009203	0.000425	0.282138	0.000030	0.282129	−22.4	0.4	1546	2208	−0.99
2	1050	0.027887	0.001089	0.282148	0.000024	0.282126	−22.1	0.3	1559	2218	−0.97
3	1050	0.031535	0.001234	0.282095	0.000030	0.282071	−23.9	−1.7	1639	2395	−0.96
4	1050	0.020556	0.000834	0.282123	0.000016	0.282106	−23.0	−0.4	1583	2281	−0.97
5	1050	0.032887	0.001285	0.282256	0.000026	0.282231	−18.3	4.0	1416	1887	−0.96
6	1050	0.033693	0.001318	0.282155	0.000025	0.282129	−21.8	0.4	1558	2208	−0.96
7	1050	0.047132	0.001801	0.282107	0.000027	0.282072	−23.5	−1.7	1647	2390	−0.95
8	1050	0.029718	0.001172	0.282356	0.000027	0.282333	−14.7	7.6	1272	1562	−0.96
9	1050	0.035414	0.001364	0.282123	0.000021	0.282097	−22.9	−0.8	1605	2312	−0.96
10	1050	0.027838	0.001086	0.282165	0.000033	0.282143	−21.5	0.9	1536	2164	−0.97
11	1050	0.031397	0.001218	0.282157	0.000030	0.282133	−21.7	0.5	1551	2196	−0.96
12	1050	0.029697	0.001193	0.282291	0.000024	0.282268	−17.0	5.3	1363	1769	−0.96
13	1050	0.023184	0.000914	0.282155	0.000028	0.282137	−21.8	0.6	1542	2185	−0.97
14	1050	0.036606	0.001455	0.282330	0.000023	0.282301	−15.6	6.5	1317	1661	−0.96
15	1050	0.046767	0.001791	0.282323	0.000036	0.282288	−15.9	6.0	1340	1705	−0.95
16	1050	0.023267	0.001002	0.282443	0.000032	0.282424	−11.6	10.8	1143	1271	−0.97
17	1050	0.036842	0.001435	0.282299	0.000034	0.282270	−16.7	5.4	1361	1760	−0.96
18	1050	0.043576	0.001609	0.282418	0.000047	0.282387	−12.5	9.5	1197	1389	−0.95
19	1050	0.026360	0.001070	0.282421	0.000024	0.282400	−12.4	9.9	1177	1348	−0.97
20	1050	0.044015	0.001577	0.282403	0.000038	0.282372	−13.1	9.0	1219	1437	−0.95
21	1050	0.132045	0.004653	0.282372	0.000083	0.282281	−14.1	5.7	1376	1727	−0.86
22	1050	0.038596	0.001495	0.282202	0.000024	0.282172	−20.2	1.9	1500	2072	−0.95
23	1050	0.023389	0.000933	0.282264	0.000032	0.282246	−18.0	4.5	1391	1838	−0.97
24	1050	0.030602	0.001190	0.282192	0.000045	0.282169	−20.5	1.8	1501	2083	−0.96
25	1050	0.020861	0.000874	0.282272	0.000042	0.282255	−17.7	4.8	1378	1810	−0.97
26	1050	0.027520	0.001085	0.282144	0.000029	0.282123	−22.2	0.1	1564	2229	−0.97
27	1050	0.036981	0.001569	0.282299	0.000035	0.282268	−16.7	5.3	1366	1769	−0.95
28	1050	0.060106	0.002330	0.282432	0.000019	0.282386	−12.0	9.4	1202	1392	−0.93
29	1050	0.032098	0.001297	0.282347	0.000031	0.282322	−15.0	7.2	1288	1596	−0.96
30	1050	0.029022	0.001165	0.282452	0.000030	0.282430	−11.3	11.0	1135	1252	−0.96
31	1050	0.027294	0.001059	0.282177	0.000023	0.282157	−21.0	1.3	1517	2122	−0.97
32	1050	0.035187	0.001363	0.282209	0.000027	0.282182	−19.9	2.2	1485	2042	−0.96
33	1050	0.026521	0.001041	0.282168	0.000030	0.282148	−21.3	1.0	1529	2150	−0.97
34	1050	0.027868	0.001085	0.282195	0.000025	0.282174	−20.4	1.9	1493	2066	−0.97

Hf_i: initial Hf isotopic compositions.

hydrothermal alteration, can be used as an alteration-independent index of geochemical variations (e.g., Polat et al., 2002). The generally immobile elements in the metabasalt samples of the Julin Group include the high field strength elements (HFSE, e.g., Nb, Ta, Ti, Hf), rare earth elements (REE), Y, Th and U. These elements are all well correlated with Zr (Fig. 8), indicating that they were essentially immobile. In contrast, the commonly mobile elements, such as Rb, Na, K, Ca, Sr and Ba, do not have co-variation with Zr (Fig. 8), suggestive of variable degree of mobility. Consequently, only the immobile elements are used for rock classification (e.g., Fig. 5) and further petrogenesis discussion.

6.2. Crystal fractionation and crustal contamination

It is generally considered that primary magmas of basaltic melts have Ni > 400 ppm and Cr > 1000 ppm (Wilson, 1989), Mg# > 73 (Sharma, 1997). The low and variable Cr and Ni concentrations and Mg# values of the metabasalts in the Julin Group suggest that the rocks were formed from highly evolved magmas which may have undergone significant fractionation of olivine and pyroxene. Most samples do not show obvious Eu anomalies, indicating that fractionation of plagioclase has been less important, consistent with minor phenocrysts of plagioclase in some slightly deformed basalts (YBGMR, 1991; Deng, 2000).

Fractional crystallization could have been accompanied by crustal contamination (AFC process) during ascending of the primary magma. Because continental crust is poor in Nb–Ta but rich in Th, Zr, Hf and light REEs, it is expected that crustal contamination of basaltic magmas would result in dramatic increase of Zr/Nb, La/Nb, Th/La, La/Sm, Th/Yb and Hf/Sm ratios (e.g., Hawkesworth et al., 1995; Ewart et al., 1998; Wang et al., 2008). Consequently, crustal contamination can produce negative correlations between Nb/La and La/Sm or Th/Ta. The variable Nb/La and Th/Ta ratios and εNd(t) and zircon εHf(t) values suggest that the basalts in this study may have undergone variable degree of crustal contamination (Figs. 7 and 9). Both La/Sm and Th/Ta are roughly negatively correlated with Nb/La, consistent with an AFC process (Fig. 9b, c). In terms of εNd(t) and εHf(t) values, there are mixing trends between the depleted mantle-derived melts and Paleoproterozoic mafic rocks (calculated back to ~1.0 Ga) in the southwestern Yangtze Block (Figs. 7 and 9a), suggesting that the primary magmas of the basalts have assimilated Paleoproterozoic rocks in the southwestern Yangtze Block. The metabasalts have limited $(Th/Yb)_{PM}$ values, close to the Paleoproterozoic mafic rocks but much lower than those of upper crust (Fig. 9d), confirming that the primary magmas may have been contaminated by some mafic rocks (Fig. 9d).

6.3. Nature of the mantle sources

Although the basaltic magmas have undergone variable degree of crustal contamination, some metabasalt samples have positive εNd(t) (up to +3.8) and zircon εHf(t) (up to +11) values that are close to the isotopic composition of depleted mantle, indicating that the primary magmas were originated from a depleted mantle source (Fig. 7a, b). The source as depleted mantle is further indicated by the low La/Ta ratios of the metabasalt samples, typically observed

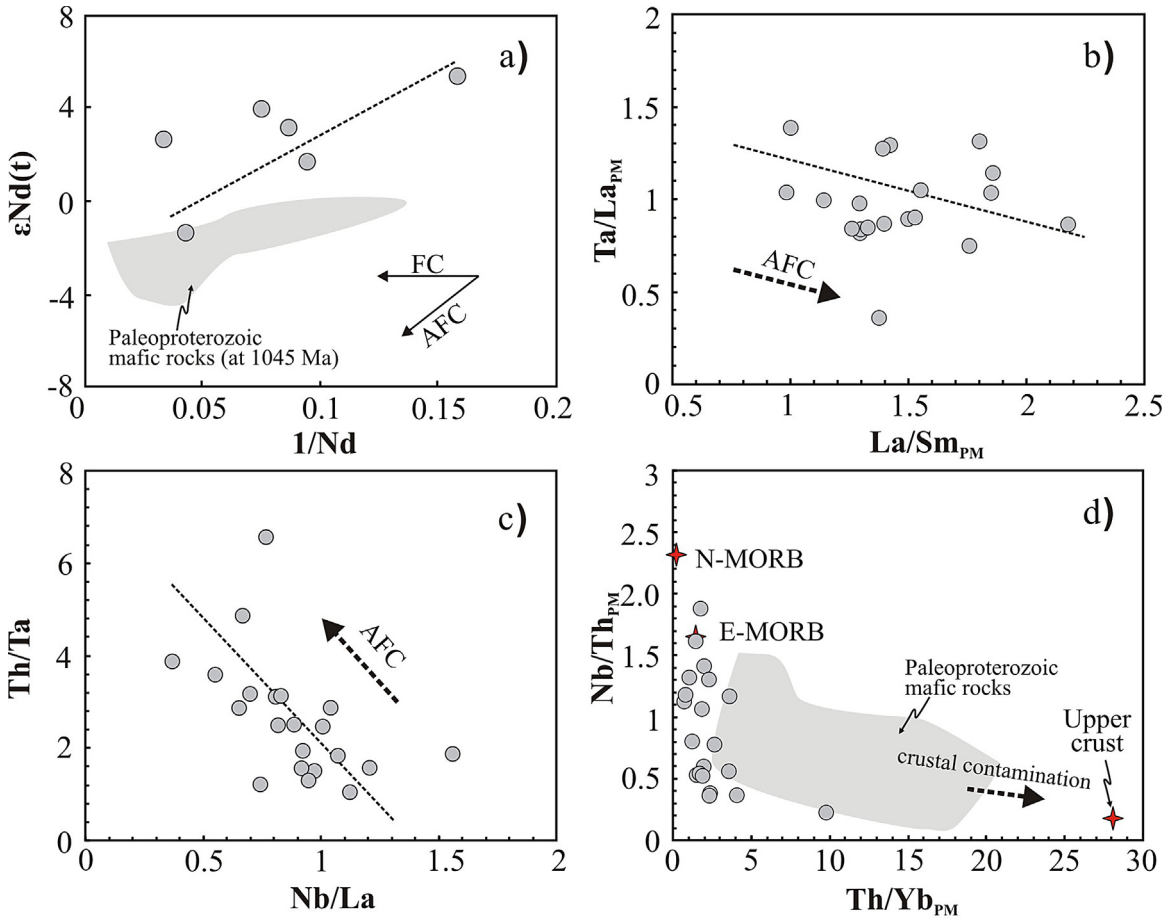

Fig. 9. Plots of εNd(t) values versus 1/Nd, Ta/La_{PM} versus La/Sm_{PM}, Th/Ta versus Nb/La and Nb/Th_{PM} versus Th/Yb_{PM} for the metabasalts in the Julin Group to understand the fractional crystallization and crustal assimilation (AFC) process. Variations of these elemental ratios suggest that the primary magmas of the metabasalts have assimilated significant crustal components including the Paleoproterozoic mafic rocks in the southwestern Yangtze Block.

in asthenospheric rather than lithospheric mantle-derived melts (Fig. 10a). The ratios of incompatible elements with similar partition coefficients (e.g., La/Ta, Th/La, Nb/La, Nb/Y) can be used to identify the mantle sources, provided that crustal contamination is insignificant during magma evolutions. In this study, samples with low La/Sm, Nb/La and Th/La are considered to primitive with least crustal contamination. These samples have relative flat chondrite-normalized REE patterns (Fig. 6), consistent with a depleted asthenospheric mantle source. Lastly, these samples have low La/Yb but high Nb/La ratios and plot in the fields of asthenospheric mantle sources, close to the plots of MORB (Fig. 10b).

6.4. Tectonic setting of the basaltic magmatism

The metabasalts of the Julin Group have relatively high TiO_2 (1.1–3.2 wt.%) and Ti/V ratios (>20) (Figs. 6 and 11), different from volcanic-arc or calc-alkaline basalts that are generally derived from subcontinental lithospheric mantle. These metabasalts are also locally associated with felsic volcanic layers in the Julin Group (Fig. 3c), forming a bimodal volcanic suite typical products of an extensional setting (YBGMR, 1991; Deng, 2000). The extensional environment could result from back-arc extension (Shinjo and Kato, 2000; Brown et al., 2002; Brewer et al., 2004), post-orogenic extension (Fan et al., 2001; Greentree et al., 2006), or continental rifting (Moraes et al., 2003; Ukstins et al., 2002; Mazzarini et al., 2004). Basalts from back-arc settings usually have geochemical characteristics between N-MORB and arc or calc-alkaline basalts, and commonly display negative Nb–Ta anomalies (Saunders and Tarney, 1984). However, the basalts in Julin are tholeiitic in compositions, with most samples lacking negative Nb–Ta anomalies (e.g., Fig. 6a and b). The metabasalts also differ from post-orogenic basalts which are commonly originated from previously-metasomatized lithospheric mantle and thus commonly exhibit negative Nb–Ta anomalies.

The metabasalt samples in the Julin Group are characterized by enrichments of incompatible elements like TiO_2 (1.1–3.2 wt.%) and HFSE (up to 40 ppm Nb) without pronounced negative

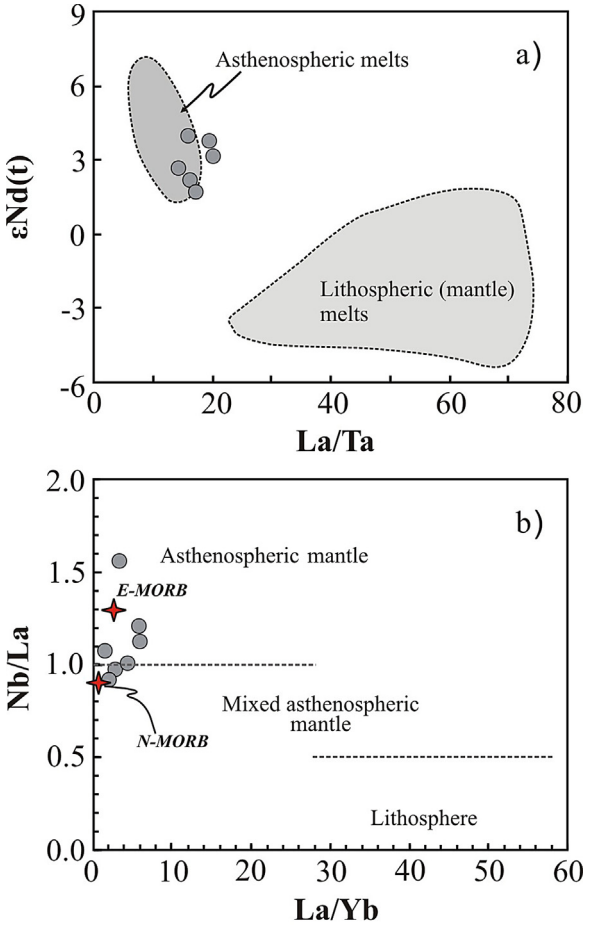

Fig. 10. Plots of elements and elemental ratios for the metabasalts to constrain the nature of the mantle source. (a) $\varepsilon Nd(t)$ versus La/Ta. The fields of the asthenospheric and lithospheric melts are from Lawton and McMillan (1999); (b) La/Yb versus Nb/La (after Watson, 1993).

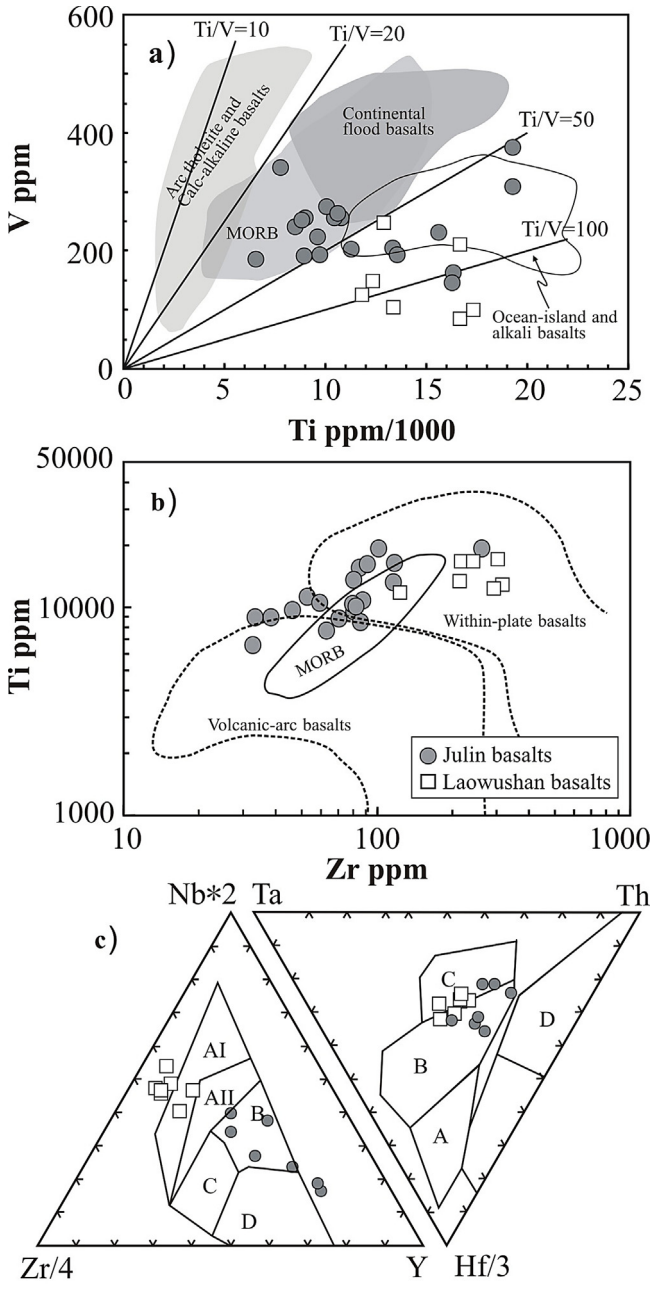

Fig. 11. Geochemical discrimination diagrams for the metabasalts in the Julin Group and Laowushan Formation (data from Greentree et al., 2006). (a) Ti versus V diagram (after Shervais, 1982); (b) Zr versus Ti diagram (after Pearce, 1982); (c) the Zr/4-Y-Nb*2 diagram is after Meschede (1986), and the fields are: AI-within-plate alkali basalts, AII-within-plate alkali basalts and tholeiites, B-E-type MORB, C-within-plate tholeiites and volcanic-arc basalts and D-N-type MORB and volcanic-arc basalts; the Th-Hf/3-Ta diagram is after Wood (1980), and the fields are: A-N-type MORB, B-E-type MORB and within-plate tholeiites, C-alkaline within-plate basalts and D-volcanic-arc basalts.

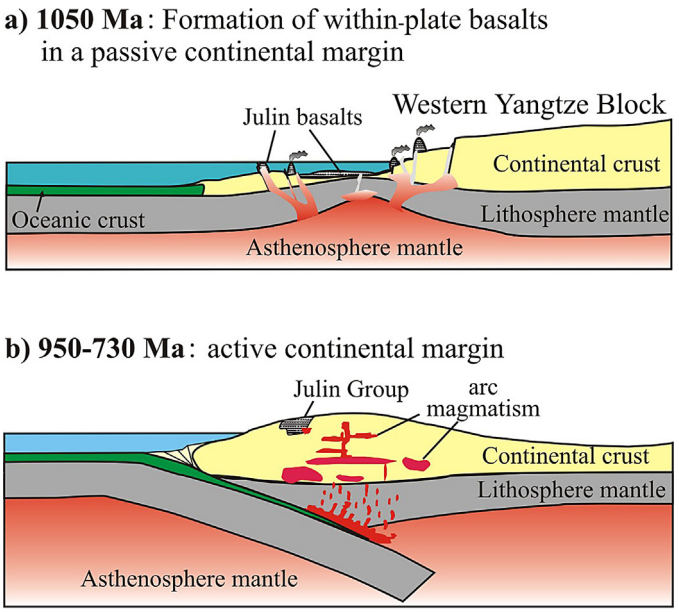

Fig. 12. A sketch cartoon showing the tectonic evolution of the western Yangtze Block from ca. 1050 Ma to 730 Ma. (a) The ~1050 Ma Julin basalts have formed in a rifting basin likely in a passive continental margin; the passive margin has evolved to be a positive margin with oceanic subduction initiating at 950 Ma; (b) long-lived oceanic subduction beneath the western margin of the Yangtze Block have produced extensive arc magmatism (950–730 Ma; Zhao and Zhou, 2007; Zhao et al., 2011).

Nb–Ta–Zr–Hf anomalies, features similar to within-plate basalts generated in a continental rift (e.g. Rogers et al., 2000; Ritter et al., 2001). Some trace element discrimination schemes, such as Ti–Zr, Hf–Th–Ta and Zr–Nb–Y diagrams, are also useful in understanding of tectonic environments of mafic rocks (Pearce and Cann, 1973; Pearce and Norry, 1979; Wood, 1980; Meschede, 1986). In the Zr–Ti diagram, the metabasalt samples plot in 'MORB' and 'within-plate basalts' fields (Fig. 11b). In the Th–Ta–Hf and Zr–Y–Nb triangle diagrams, the samples with minor crustal contamination mostly plot in the 'E-type MORB and within-plate tholeiites' field, a feature similar to the ca. 1142 Ma Laowushan alkaline basalts (Fig. 11c). Furthermore, coeval felsic volcanic rocks in the upper part of the Huili Group have geochemical affinity of A-type granites, consistent with an intra-plate rifting setting (Geng et al., 2007). Collectively, it is concluded that the basaltic rocks have formed in a continental rift.

Formation of the basaltic layers in the Pudeng Formation was followed by depositions of massive sandstone of the Lugumo Formation and subsequently massive marble (or dolomite) of the Fenghuangshan Formation of the Julin Group. Similar sedimentary sequences is also present in the Limahe and Fengshanying formations of the coeval Huili Group. These sedimentary sequences have been suggested to be related to a shallow marine environment in a rifting basin (Fig. 12a) (YBGMR, 1991; Deng, 2000).

6.5. *Grenvillian intra-plate magmatism in the southwestern Yangtze Block*

Our investigations demonstrate that the ca. 1050 Ma basalts in the Julin Group represent intra-plate magmatism generated in a continental rift. Other studies have also identified Mesoproterozoic magmatism in the southwestern Yangtze Block, including the ca. 1142 Ma Laowushan alkaline basalts (Greentree et al., 2006), the ca. 1028 Ma Tianbaoshan alkaline felsic volcanic rocks (Geng et al., 2007) and the ca. 1063 Ma Tangtang A-type granite (Wang et al., 2012a,b). It is concluded that these magmatic rocks have formed in intra-plate rifting rather than orogenic setting in the

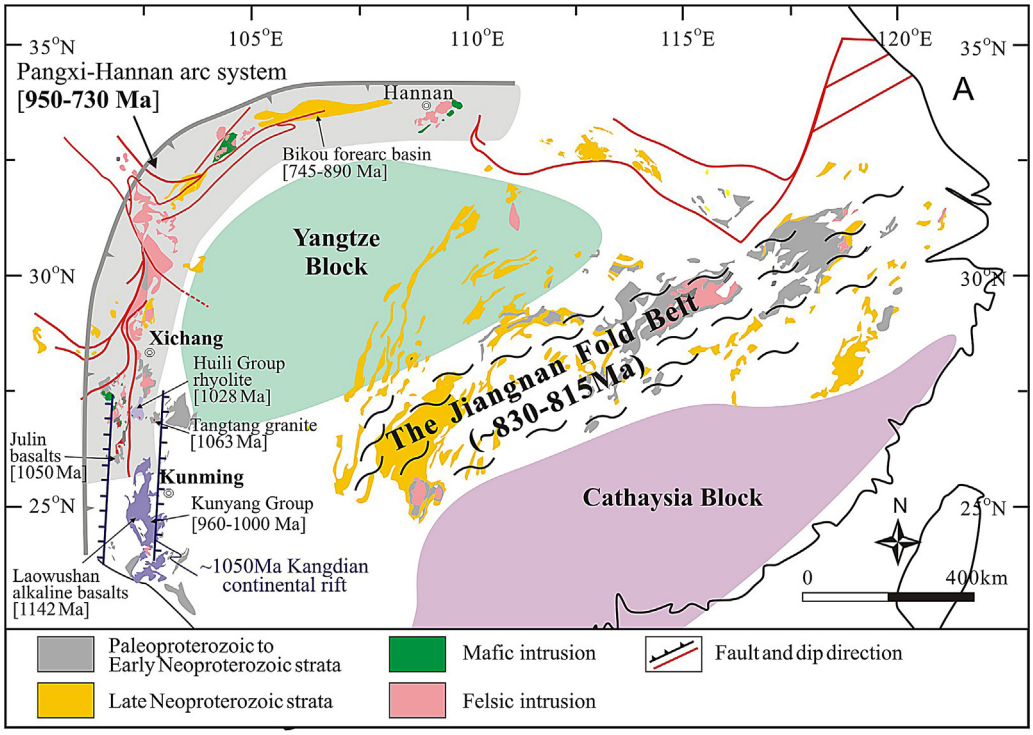

Fig. 13. A sketch geological map showing the Precambrian tectonic evolution of the South China Craton. Note that the timing of the Sibao/Jiangnan orogen is now constrained to be about 830–815 Ma. In the western Yangtze Block, the ~1140 to ~1000 Ma igneous and sedimentary rocks have formed in a rifting basin likely in a passive continental margin. Subsequently, the passive margin has evolved to be a positive margin with oceanic subduction initiating at 950 Ma, which likely indicate the onset of the amalgamation of the Yangtze Block with other blocks in the Rodinia supercontinent. Age data for the Mesoproterozoic strata and igneous rocks in the southwestern Yangtze Block are from Greentree et al. (2006), Geng et al. (2007), Sun et al. (2009) and Wang et al. (2012c).

southwestern Yangtze Block during the period of ~1150 to ~1000 Ma (Fig. 13), arguing against the existence of a Grenvillian orogenic belt that has been traditionally thought to extend from the southeast (e.g., Fig. 1; Li et al., 1999, 2002a; Greentree et al., 2006). In fact, recent dating results have demonstrated that the so-called Sibao Orogen in the southeastern Yangtze Block formed in Neoproterozoic rather than Mesoproterozoic (Greenville) (Zhao et al., 2011; Wang et al., 2012a,b, 2013; Zhang et al., 2012). Widely distributed metasedimentary rocks which was previously thought to be Mesoproterozoic have been recently demonstrated to be Neoproterozoic (830–815 Ma) and formed in back-arc to retroarc foreland basin related to the orogen (Gao et al., 2008; Wang et al., 2010, 2012a,b, 2013; Zhao et al., 2011). New radiometric data also suggest that the ophiolitic complex in southern Anhui Province was emplaced at ca. 824 Ma, representing the timing of the arc-continental collision (Zhang et al., 2012). All these data confirm that the so-called Sibao Orogen is Neoproterozoic (830–815 Ma) in age and unlikely to be part of Greenville orogenic belt in the world.

In the southwestern Yangtze Block, widespread mid-Neoproterozoic mafic and felsic igneous assemblages (ca. 860–740 Ma) have been interpreted as the products of a mantle plume (Li et al., 1995, 1999) or of oceanic subduction (Zhou et al., 2002a,b). The 'mantle plume' model was largely based on the assumption that the arc signature of these Neoproterozoic igneous rocks was inherited from mantle sources previously modified by oceanic subduction related to the Grenvillian orogeny (e.g., Li et al., 1999; Wang et al., 2008). However, results from this study argue against a Grenvillian orogen in the southwestern Yangtze Block. In addition, numerous studies on detrital zircon of sedimentary rocks and geochemistry of igneous rocks indicate that the Neoproterozoic igneous rocks recorded a prolonged magmatic history from ca. 950 to 740 Ma related to a continental magmatic arc in the western Yangtze Block (e.g., the Panxi-Hannan arc belt; Zhou et al., 2002b, 2006; Sun et al., 2008, 2009; Zhao et al., 2011). This long-lived magmatic system is best represented by the 950–900 Ma Xixiang basalts (Ling et al., 2003), the 820–746 Ma Hannan mafic-ultramafic intrusions (Zhou et al., 2002a; Zhao and Zhou, 2009), and the 846–776 Ma Bikou volcanic rocks (Yan et al., 2004) in the northwestern Yangtze Block, and the 740 Ma Panzhihua gabbroic and 760 Ma Datian adakitic intrusions (Zhao and Zhou, 2007) in the western Yangtze Block.

The late Mesoproterozoic within-plate magmatism and subsequent early Neoproterozoic arc magmatic activities in the southwestern Yangtze Block thus suggest that the late Mesoproterozoic Julin Group and the other equivalents in this region have formed at an intra-continental rifting basin in a passive margin. The passive margin has evolved to be a positive margin with oceanic subduction initiating at 950 Ma (Fig. 12) (Zhou et al., 2002a; Zhao and Zhou, 2007; Zhao et al., 2011). This tectonic switch likely indicate the onset of the amalgamation of the Yangtze Block with other blocks in the Rodinia supercontinent (Zhou et al., 2002b; Zhao and Zhou, 2009). This interpretation argues against the view that the Yangtze Block is in the interior of the Rodinia supercontinent based on the assumed Grenvillian orogeny in South China (Li et al., 1995, 2002a; Piper, 2000; Jiang et al., 2003; Meert and Torsvik, 2003; Yu et al., 2008; Qiu et al., 2011). In contrast, this study supports the model that the Neoproterozoic Panxi-Hannan arc belt may be part of a magmatic belt along the western margin of East Gondwana and Australia, and thus the Yangtze Block was possibly located along the margin of the Rodinia supercontinent (Zhao and Zhou, 2007; and reference therein).

7. Conclusions

1. The ~1050 Ma metabasalts in the Julin Group in the southwestern margin of the Yangtze Block have tholeiitic compositions, and were derived from a depleted asthenospheric mantle source followed by significant fractional crystallization and crustal contaminations during magma ascending.
2. The metabasalts in the Julin Group have geochemical affinity of within-plate basalts. They have formed in a continental rift, similar to the contemporary igneous rocks in the same region, recording a ~1050 Ma rifting event in the southwestern the Yangtze Block.
3. Both the metabasalts and associated sedimentary rocks in the Julin Group indicate a shallow marine environment likely on a passive continental margin. This study does not support the existence of a Grenvillian orogenic belt in the southwestern Yangtze Block, and thus there is no evidence that the Yangtze Block was located in the interior of the Rodinia supercontinent.

Acknowledgements

This study is supported by the National Natural Science Foundation of China (Grant 41172174/D0210 and 41272212) and grants from the Research Grant Council of Hong Kong (HKU707210P and HKU707511P). We thank Mr. Ying Zhang and Dr. Xinfu Zhao for helping with our field work. Prof. Liang Qi, Ms. Xiao Fu, Ms. Yang Yang are greatly appreciated for their assistances with the analyses. We are grateful to the official reviews by two anonymous reviewers and editorial handling by Editor Prof GC Zhao.

References

Amelin, Y., Lee, D.-C., Halliday, A.N., Pidgeon, R.T., 1999. Nature of the Earth's earliest crust from hafnium isotopes in single detrital zircons. Nature 399, 252–255.
BGMRSP (Bureau of Geology and Mineral Resources of the Sichuan Province), 1970. Regional geological survey of People's Republic of China: the Huili Sheet (G-48-XIII; geological part), scale 1: 200,000 (in Chinese).
Blichert-Toft, J., Albarède, F., 1997. The Lu–Hf isotope geochemistry of chondrites and the evolution of the mantle-crust system. Earth and Planetary Science Letters 148, 243–258.
Boger, S.D., Wilson, C.J.L., Fanning, C.M., 2001. Early Paleozoic tectonism within the East Antarctic Craton: the final suture between East and West Gondwana? Geology 29, 463–466.
Brewer, T.S., Ahall, K.I., Menuge, J.F., Storey, C.D., Parrish, R.R., 2004. Mesoproterozoic bimodal volcanism in SW Norway, evidence for recurring pre-Sveconorwegian continental margin tectonism. Precambrian Research 134, 249–273.
Brown, S.J.A., Barley, M.E., Krapez, B., Cas, R.A.F., 2002. The Late Archaean Melita Complex, Eastern Goldfields, Western Australia: shallow submarine bimodal volcanism in a rifted arc environment. Journal of Volanology and Geothermal Research 115, 303–327.
Burrett, C., Berry, R., 2000. Proterozoic Australia–Western United States (AUSWUS) fit between Laurentia and Australia. Geology 28, 103–106.
Chauvel, C., Bureau, S., Poggi, C., 2011. Comprehensive chemical and analyses of basalt and sediment reference materials. Geostandards and Geoanalytical Research 35, 125–143.
Chen, W.T., Zhou, M.F., Zhao, X.F., 2013. Late Paleoproterozoic sedimentary and mafic rocks in the Hekou area, SW China: implication for the reconstruction of the Yangtze Block in Columbia. Precambrian Research 231, 61–77.
Chen, Z.L., Chen, S.Y., 1987. On the Tectonic Evolution of the West Margin of the Yangzi Block. Chongqing Publishing House, Chongqing, China, pp. 172 (in Chinese with English abstract).
Chu, N.C., Taylor, R.N., Chavagnac, V., Nesbitt, R.W., Boella, R.M., Milton, J.A., German, C.R., Bayon, G., Burton, K., 2002. Hf isotope ratio analysis using multi-collector inductively coupled plasma mass spectrometry: an evaluation of isobaric interference corrections. Journal of Analytical Atomic Spectrometry 17, 1567–1574.
Clarke, G.L., Sun, S.S., White, R.W., 1995. Grenville age belts and adjacent older terranes in Australia and Antarctica. AGSO Journal of Australian Geology and Geophysics 16, 25–39.
Deng, S.X., (Unpublished Ph.D. thesis) 2000. The evolution of metamorphism and geochemistry for the Cangshan and Julin Groups in Central Yunnan, China. Guangzhou Institute of Geochemistry, Chinese Academy of Sciences, pp. 41–49 (in Chinese with English abstract).
Ewart, A., Milner, S.C., Armstrong, R.A., Duncan, A.R., 1998. Etendeka volcanism of the Goboboseb mountains and Messum igneous complex, Namibia. Part I: Geochemical evidence of early Cretaceous Tristan Plume melts and the role of crustal contamination in the Parana-Etendeka CFB. Journal of Petrology 39 (2), 191–225.
Fan, W.M., Guo, F., Wang, Y.J., Lin, G., Zhang, M., 2001. Post-orogenic bimodal volcanism along the Sulu Orogenic Belt in Eastern China. Physics and Chemistry of the Earth (A) 26 (9–10), 133–146.
Gao, L.Z., Yang, M.G., Ding, X.Z., Liu, Y.X., Liu, X., Ling, L.H., Zhang, C.H., 2008. SHRIMP U–Pb zircon dating of tuff in the Shuangqiaoshan and Heshangzhen groups in

South China-constraints on the evolution of the Jiangnan Neoproterozoic orogenic belt. Geological Bulletin of China 27, 1744–1751 (in Chinese with English Abstract).
Gao, S., Yang, J., Zhou, L., Li, M., Hu, Z., Guo, J., Yuan, H., Gong, H., Xiao, G., Wei, J., 2011. Age and growth of the Archean Kongling terrain, South China, with emphasis on 3.3 Ga granitoid gneisses. American Journal of Science 311, 153–182.
Geng, Y., Yang, C., Du, L., Wang, X., Ren, L., Zhou, X., 2007. Chronology and tectonic environment of the Tianbaoshan Formation: new evidence from zircon SHRIMP U–Pb age and geochemistry. Geological Review 53, 556–563 (in Chinese with English abstract).
Greentree, M.R., Li, Z.X., 2008. The oldest known rocks in south-western China: SHRIMP U–Pb magmatic crystallisation age and detrital provenance analysis of the Paleoproterozoic Dahongshan Group. Journal of Asian Earth Sciences 33, 289–302.
Greentree, M.R., Li, Z.X., Li, X.H., Wu, H., 2006. Late Mesoproterozoic to earliest Neoproterozoic basin record of the Sibao orogenesis in western South China and relationship to the assembly of Rodinia. Precambrian Research 151, 79–100.
Griffin, W.L., Pearson, N.J., Belousova, E., Jackson, S.E., van Achterbergh, E., Reilly, S.Y., Shee, S.R., 2000. The Hf isotope composition of cratonic mantle: LAM-MC-ICPMS analysis of zircon megacrysts in kimberlites. Geochimica et Cosmochimica Acta 64 (1), 133–147.
Guan, J.L., Zheng, L.L., Lui, J.H., Sun, Z.M., Cheng, W.H., 2011. Zircons SHRIMP U–Pb dating of diabase from Hekou, Sichuan Province, China and its geological significance. Acta Geologica Sinica 85 (4), 482–490 (in Chinese with English abstract).
Hawkesworth, C.J., Lightfoot, P.C., Fedorenko, V.A., Blake, S., Naldrett, A.J., Doherty, W., Gorbachev, N.S., 1995. Magma differentiation and mineralisation in the Siberian continental flood basalts. Lithos 34, 61–88.
Hoffman, P., 1991. Did the breakout of Laurentia turn Gondwanaland inside-out? Science 252, 1409.
Hu, A., Zhu, B., Mao, C., Zhu, N., Hunang, R., 1991. Geochronology of the Dahongshan Group. Chinese Journal of Geochemistry 10 (3), 195–203.
Huang, X.L., Xu, Y.G., Lan, J.B., Yang, Q.J., Luo, Z.Y., 2009. Neoproterozoic adakitic rocks from Mopanshan in the western Yangtze Craton: partial melts of a thickened lower crust. Lithos 112, 367–381.
Huang, X.L., Xu, Y.G., Li, X.H., Li, W.X., Lan, J.B., Zhang, H.H., Liu, Y.S., Wang, Y.B., Li, H.Y., Luo, Z.Y., Yang, Q.J., 2008. Petrogenesis and tectonic implications of Neoproterozoic, highly fractionated A-type granites from Mianning, South China. Precambrian Research 165, 190–204.
Jacobs, J., Fanning, C.M., Bauer, W., 2003. Timing of Grenville-age vs. Pan-African medium- to high grade metamorphism in western Dronning Maud Land (East Antarctica) and significance for correlations in Rodinia and Gondwana. Precambrian Research 125, 1–20.
Jackson, S.E., Pearson, N.J., Griffin, W.L., Belousova, E.A., 2004. The application of laser ablation-inductively coupled plasma-mass spectrometry to *in situ* U–Pb zircon geochronology. Chemical Geology 211, 47–69.
Jiang, G., Sohl, L.E., Christie-Blick, N., 2003. Neoproterozoic stratigraphic comparison of the Lesser Himalaya (India) and Yangtze block (South China): paleogeographic implications. Geology 31, 917–920.
Karlstrom, K.E., Åhäll, K.-I., Harlan, S.S., Williams, M.L., McLelland, J., Geissman, J.W., 2001. Long-lived (1.8–1.0 Ga) convergent orogen in southern Laurentia, its extensions to Australia and Baltica, and implications for refining Rodinia. Precambrian Research 111, 5–30.
Lawton, T.F., McMillan, N.J., 1999. Arc abandonment as a cause for passive continental rifting: comparison of the Jurassic Mexican Borderland rift and the Cenozoic Rio Grande rift. Geology 27, 779–782.
Li, F.H., Tan, J.M., Shen, Y.L., Yu, F.X., Zhou, G.F., Pan, X.N., Li, X.Z., 1988. The Presinian in the Kangdian Area. Chongqing Publishing House, Chongqing, China, pp. 396 (in Chinese with English abstract).
Li, L.M., Lin, S., Xing, G., Davis, D.W., Davis, W.J., Xiao, W., Yin, C., 2013. Geochemistry and tectonic implications of late Mesoproterozoic alkaline bimodal volcanic rocks from the Tieshanjie Group in the southeastern Yangtze Block, South China. Precambrian Research 230, 179–192.
Li, X.H., Li, Z.X., Zhou, H., Liu, Y., Kinny, P.D., 2002b. U–Pb zircon geochronology, geochemistry and Nd isotopic study of Neoproterozoic bimodal volcanic rocks in the Kangdian Rift of South China: implications for the initial rifting of Rodina. Precambrian Research 113, 135–154.
Li, X.H., Li, W.X., Li, Z.X., Lo, C.H., Wang, J., Ye, M.F., Yang, Y.H., 2009. Amalgamation between the Yangtze and Cathaysia blocks in South China: constraints from SHRIMP U–Pb zircon ages, geochemistry and Nd–Hf isotopes of the Shuangxiwu volcanic rocks. Precambrian Research 174, 117–128.
Li, X.H., Liu, D.Y., Sun, M., Li, W.X., Liang, X.R., Liu, Y., 2004. Precise Sm–Nd and U–Pb isotopic dating of the super-giant Shizhuyuan polymetallic deposit and its host granite, Southeast China. Geological Magazine 141, 225–231.
Li, Z.X., Bogdanova, S.V., Collins, A.S., Davidson, A., De Waele, B., Ernst, R.E., Fitzsimons, I.C.W., Fuck, R.A., Gladkochub, D.P., Jacobs, J., Karlstrom, K.E., Lu, S., Natapov, L.M., Pease, V., Pisarevsky, S.A., Thrane, K., Vernikovsky, V., 2008. Assembly, configuration, and break-up history of Rodinia: a synthesis. Precambrian Research 160, 179–210.
Li, Z.X., Li, X.H., Kinny, P.D., Wang, J., Zhang, S., Zhou, H., 2003. Geochronology of Neoproterozoic syn-rift magmatism in the Yangtze Craton, South China and correlations with other continents. evidence for a mantle superplume that broke up Rodinia. Precambrian Research 122, 85–109.
Li, Z.X., Li, X.H., Kinny, P.D., Wang, J., 1999. The breakup of Rodinia: did it start with a mantle plume beneath South China? Earth and Planetary Science Letters 173, 171–181.
Li, Z.-X., Li, X.-H., Zhou, H., Kinny, P.D., 2002a. Grenvillian continental collision in south China: new SHRIMP U–Pb zircon results and implications for the configuration of Rodinia. Geology 30, 163–166.
Li, Z.X., Wartho, J.A., Occhipinti, S., Zhang, C.L., Li, X.H., Wang, J., Bao, C.M., 2007. Early history of the eastern Sibao Orogen (South China) during the assembly of Rodinia: new mica $^{40}Ar/^{39}Ar$ dating and SHRIMP U–Pb detrital zircon provenance constraints. Precambrian Research 159, 79–94.
Li, Z.X., Zhang, L., Powell, C.M., 1995. South China in Rodinia: part of the missing link between Australia–East Antarctica and Laurentia? Geology 23, 407–410.
Ling, W.L., Gao, S., Zhang, B.R., Li, H.M., Liu, Y., Cheng, J.P., 2003. Neoproterozoic tectonic evolution of the northwestern Yangtze craton, South China: implications for amalgamation and break-up of the Rodinia Supercontinent. Precambrian Research 122, 111–140.
Liu, Y.S., Hu, Z.C., Gao, S., Gunther, D., Xu, J., Gao, C.G., Chen, H.H., 2008. In situ analysis of major and trace elements of anhydrous minerals by LA-ICP-MS without applying an internal standard. Chemical Geology 257, 34–43.
Ludwig, K.R., 2003. Isoplot 3.00: A Geochronological Toolkit for Microsoft Excel. Berkeley Geochronology Center, Berkeley, CA.
Machado, N., Simonetti, A., 2001. U–Pb dating and Hf isotopic composition of zircons by laser ablation-MC-ICP-MSA. In: Sylverster, P. (Ed.), Laser Ablation ICPMS in the Earth Sciences: Principles and Applications, Short Course, vol. 29. Mineralogical Association of Canada, pp. 121–146.
Mazzarini, F., Corti, G., Manetti, P., Innocenti, F., 2004. Strain rate and bimodal volcanism in the continental rift: Debre Zeyt volcanic field, northern MER, Ethiopia. Journal of African Earth Sciences 39, 415–420.
Meert, J.G., Torsvik, T.H., 2003. The making and unmaking of a supercontinent: Rodinia revisited. Tectonophysics 375, 261–288.
Meschede, M., 1986. A method of discrimination between different types of mid-oceanic ridge basalts and continental tholeiites with the Nb–Zr–Y diagram. Chemical Geology 56, 207–218.
Miyashiro, A., 1974. Volcanic rock series in island arcs and active continental margins. American Journal of Science 274 (4), 321–355.
Moraes, R., Fuck, R.A., Pimentel, M.M., Gioia, S.M.C.L., Figueiredo, A.M.G., 2003. Geochemistry and Sm–Nd isotopic characteristics of bimodal volcanic rocks of Juscelandia, Goiás Brazil: mesoproterozoic transition from continental rift to ocean basin. Precambrian Research 125, 317–336.
Pearce, J.A., 1982. Trace element characteristics of lavas from destructive plate boundaries. In: Thorpe, R.S. (Ed.), Andesites: Orogenic Andesites and Related Rocks. Wiley, Chichester, pp. 525–548.
Pearce, J.A., Cann, J.R., 1973. Tectonic setting of basic volcanic rocks using determined using trace element analysis. Earth and Planetary Science Letter 19, 290–300.
Pearce, J.A., Norry, M.J., 1979. Petrogenetic implications of Ti, Zr, Y, and Nb variations in volcanic rocks. Contributions to Mineralogy and Petrology 69, 33–47.
Peng, M., Wu, Y.B., Wang, J., Jiao, W.F., Liu, X.C., Yang, S.H., 2009. Paleoproterozoic mafic dyke from Kongling terrain in the Yangtze Craton and its implication. Chinese Science Bulletin 54 (6), 1098–1104.
Piper, J.D.A., 2000. The Neoproterozoic supercontinent: Rodinia or Palaeopangea? Earth and Planetary Science Letter 176, 131–146.
Polat, A., Hofmann, A.W., Rosing, M.T., 2002. Boninite-like volcanic rocks in the 3.7–3.8 Ga Isua greenstone belt, West Greenland: geochemical evidence for intra-oceanic subduction zone processes in the early Earth. Chemical Geology 184, 231–254.
Qi, L., Hu, J., Gregoire, D.C., 2000. Determination of trace elements in granites by inductively coupled plasma-mass spectrometry. Talanta 51, 507–513.
Qiu, X.F., Ling, W.L., Liu, X.M., Kusky, T., Berkana, W., Zhang, Y.H., Gao, Y.J., Lu, S.S., Kuang, H., Liu, C.X., 2011. Recognition of Grenvillian volcanic suite in the Shennongjia region and its tectonic significance for the South China Craton. Precambrian Research 191, 101–119.
Qiu, Y.M., Gao, S., McNaughton, N.J., Groves, D.I., Ling, W., 2000. First evidence of >3.2 Ga continental crust in the Yangtze craton of South China and its implications for Archean crustal evolution and Phanerozoic tectonics. Geology 28 (1), 11–14.
Ritter, J.R.R., Jordan, M., Christensen, U.R., Achauer, U., 2001. A mantle plume below the Eifil volcanic fields, Germany. Earth and Planetary Science Letters 186, 7–14.
Rogers, N., Macdonald, R., Fitton, J.G., George, R., Smith, M., Barreiro, B., 2000. Two mantle plumes beneath the East African rift system: Sr, Nd, and Pb isotope evidence from Kenya Rift basalts. Earth and Planetary Science Letters 176, 387–400.
Saunders, A.D., Tarney, J., 1984. Geochemical characteristics of basaltic volcanism within back-arc basins. Geological Society, London (Special Publications) 16, 59–76.
Scherer, E., Munker, C., Mezger, K., 2001. Calibration of the lutetium–hafnium clock. Science 293, 683–687.
Sharma, M., 1997. Siberian traps. In: Mahoney, J.J., Coffin, M.F. (Eds.), Large Igneous Provinces: Continental, Oceanic, and Planetary Flood Volcanism, vol. 100. American Geophysical Union Geophysical Monograph, pp. 273–295.
Shervais, J.W., 1982. Ti–V plots and the petrogenesis of modern ophiolitic lavas. Earth and Planetary Science Letter 59, 101–118.
Shinjo, R., Kato, Y., 2000. Geochemical constraints on the origin of bimodal magmatism at the Okinawa Trough, an incipient back-arc basin. Lithos 54, 117–137.
Sun, S.S., McDonough, W.F. (Eds.), 1989. In: Magmatism in the Ocean Basins, vol. 42. Geological Society Special Publication.
Sun, W.H., Zhou, M.F., 2008. The ~860-Ma, Cordilleran-Type Guandaoshan Dioritic Pluton in the Yangtze Block, SW China: implications for the origin of Neoproterozoic magmatism. The Journal of Geology 116, 238–253.
Sun, W.H., Zhou, M.F., Gao, J.F., Yang, Y.H., Zhao, X.F., Zhao, J.H., 2009. Detrital zircon U–Pb geochronological and Lu–Hf isotopic constraints on the Precambrian

magmatic and crustal evolution of the western Yangtze Block, SW China. Precambrian Research 172, 99–126.
Sun, W.H., Zhou, M.F., Yan, D.P., Li, J.W., Ma, Y.X., 2008. Provenance and tectonic setting of the Neoproterozoic Yanbian Group, western Yangtze Block (SW China). Precambrian Research 167, 213–236.
Ukstins, I.A., Renne, P.R., Wolfenden, E., Baker, J., Ayalew, D., Menzies, M., 2002. Matching conjugate volcanic rifted margins: $^{40}Ar/^{39}Ar$ chrono-stratigraphy of pre- and syn-rift bimodal food volcanism in Ethiopia and Yemen. Earth and Planetary Science Letters 198, 289–306.
Wang, J., Li, Z.X., 2003. History of Neoproterozoic rift basins in South China: implications for Rodinia break-up. Precambrian Research 122, 141–158.
Wang, W., Wang, F., Chen, F., Zhu, X., Xiao, P., Siebel, W., 2010. Detrital zircon ages and Hf–Nd isotopic composition of Neoproterozoic sedimentary rocks in the Yangtze Block: constraints on the deposition age and provenance. The Journal of Geology 118, 79–94.
Wang, W., Zhou, M.-F., 2012. Sedimentary records of the Yangtze Block (South China) and their correlation with equivalent Neoproterozoic sequences on adjacent continents. Sedimentary Geology 265–266, 126–142.
Wang, W., Chen, F.K., Hu, R., Chu, Y., Yang, Y.Z., 2012a. Provenance and tectonic setting of Neoproterozoic sedimentary sequences in the South China Block: evidence from detrital zircon ages and Hf–Nd isotopes. International Journal of Earth Sciences 101, 1723–1744.
Wang, W., Zhou, M.-F., Yan, D.-P., Li, J.-W., 2012b. Depositional age, provenance, and tectonic setting of the Neoproterozoic Sibao Group, southeastern Yangtze Block, South China. Precambrian Research 192–195, 107–124.
Wang, W., Zhou, M.F., Yan, D.P., Li, L., John, M., 2013. Detrital zircon record of Neoproterozoic active-margin sedimentation in the eastern Jiangnan Orogen, South China. Precambrian Research 235, 1–19.
Wang, X.C., Li, X.H., Li, Z.X., Liu, Y., Liu, Y., Yang, Y.H., Liang, X.-R., Tu, X.-L., 2008. The Bikou basalts in the northwestern Yangtze block, South China: remnants of 820–810 Ma continental flood basalts? Geological Society of America Bulletin 120, 1478–1492.
Wang, Z., Zhou, B., Guo, Y., Yang, B., Liao, Z., Wang, S., 2012c. Geochemistry and zircon U–Pb dating of Tangtang granite in the western margin of the Yangtze Platform. Acta Petrologica et Mineralogica 31, 652–662 (in Chinese with English abstract).
Watson, S., 1993. Rare earth element inversions and percolation models for Hawaii. Journal of Petrology 34, 763–783.
Wiedenbeck, M., Alle, P., Corfu, F., Griffin, W.L., Meier, M., Oberli, F., Vonquadt, A., Roddick, J.C., Speigel, W., 1995. Three natural zircon standards for U–Th–Pb, Lu–Hf, trace-element and REE analyses. Geostandards Newsletter 19, 1–23.
Wilson, M., 1989. Igneous Petrogenesis. Chapman & Hall, London, pp. 466.
Winchester, J.A., Floyd, P.A., 1976. Geochemical magma type discrimination: application to altered and metamorphosed basic igneous rocks. Earth and Planetary Science Letters 28, 459–469.
Winchester, J.A., Floyd, P.A., 1977. Geochemical discrimination of different magma series and their differentiation products using immobile elements. Chemical Geology 20, 325–343.
Wood, D.A., 1980. The application of a Th–Hf–Ta diagram to problems of tectonomagmatic classification and to establishing the nature of crust contamination of basaltic lavas of the British Tertiary volcanic province. Earth and Planetary Science Letters 50, 11–30.
Wu, M.D., Duan, J.S., Song, X.L., Chen, L., Dan, Y., 1990. Geology of Kunyang Group in Yunnan Province. Scientific Press of Yunnan Province, Kunming, pp. 265 (in Chinese with English abstract).
Xiong, Q., Zheng, J.P., Yu, C.M., Su, Y.P., Tang, H.Y., Zhang, Z.H., 2009. Zircon U–Pb age and Hf isotope of Quanyishang A-type granite in Yichang: signification for the Yangtze continental cratonization in Paleoproterozoic. Chinese Science Bulletin 54 (3), 436–446.
Yan, Q., Hanson, A.D., Wang, Z.Q., Druschke, A.P., Yan, Z., Wang, T., Liu, D., Song, B., Jian, P., Zhou, H., Jiang, C., 2004. Neoproterozoic subduction and rifting on the northern margin of the Yangtze Plate, China: implications for Rodinia reconstruction. International Geology Review 46, 817–832.
Yang, C.H., Geng, Y.S., Du, L.L., Ren, L.D., Wang, X.S., Zhou, X.W., Yang, Z.S., 2009. The identification of the Grenvillian granite on the western margin of the Yangtze Block and its geological implications. Geology in China 36, 647–657 (in Chinese with English Abstract).
Yang, H., Liu, F.L., Du, L.L., Liu, P.H., Wang, F., 2012. Zircon U–Pb dating for metavolcanites in the laochanghe Formation of the Dahongshan Group in southwestern Yangtze Block, and its geological significance. Acta Petrologica Sinica 28 (9), 2994–3014 (in Chinese with English abstract).
YBGMR (Yunnan Bureau of Geology and Mineral Resources), 1991. Regional Geology of Yunnan Province. Geological Publishing House, Beijing (in Chinese).
Ye, M.F., Li, X.H., Li, W.X., Liu, Y., Li, Z.X., 2007. SHRIMP zircon U–Pb geochronological and whole-rock geochemical evidence for an early Neoproterozoic Sibaoan magmatic arc along the southeastern margin of the Yangtze block. Gondwana Research 12, 144–156.
Yu, J.H., O'Reilly, S.Y., Wang, L.J., Griffin, W.L., Zhang, M., Wang, R.C., Jiang, S.Y., Shu, L.S., 2008. Where was South China in the Rodinia supercontinent? Evidence from U–Pb ages and Hf isotopes of detrital zircons. Precambrian Research 164, 1–15.
Zhang, C.J., Gao, L.Z., Wu, Z.J., Shi, X.Y., Yan, Q.R., Li, D.J., 2007. SHRIMP U–Pb zircon age of tuff from the Kunyang Group in central Yunnan: evidence for Grenvillian orogeny in South China. Chinese Science Bulletin 52, 1517–1525.
Zhang, L.J., Ma, C.Q., Wang, L.X., She, Z.B., Wang, S.M., 2011. Discovery of Paleoproterozoic rapakivi granite on the northern margin of the Yangtze block and its geological significance. Chinese Science Bulletin 56 (3), 306–318.
Zhang, Q.R., Chu, X.L., Bahlburg, H., Feng, L.J., Dobrzinski, N., Zhang, T., 2003. Stratigraphic architecture of the Neoproterozoic glacial rocks in the Xiang-Qian-Gui region of the central Yangtze Block, South China. Progress in Natural Science 13, 783–787.
Zhang, S.B., Wu, R.X., Zheng, Y.F., 2012. Neoproterozoic continental accretion in South China: geochemical evidence from the Fuchuan ophiolite in the Jiangnan orogen. Precambrian Research 220–221, 45–64.
Zhao, J.H., Zhou, M.F., 2007. Geochemistry of Neoproterozoic mafic intrusions in the Panzhihua district (Sichuan Province, SW China): implications for subduction-related metasomatism in the upper mantle. Precambrian Research 152, 27–47.
Zhao, J.H., Zhou, M.F., 2009. Secular evolution of the Neoproterozoic lithospheric mantle underneath the northern margin of the Yangtze Block, South China. Lithos 107, 152–168.
Zhao, J.H., Zhou, M.F., Yan, D.P., Yang, Y.H., Sun, M., 2008. Zircon Lu–Hf isotopic constraints on Neoproterozoic subduction-related crustal growth along the western margin of the Yangtze Block, China. Precambrian Research 163, 189–209.
Zhao, J.H., Zhou, M.F., Yan, D.P., Zheng, J.P., Li, J.W., 2011. Reappraisal of the ages of Neoproterozoic strata in South China: no connection with the Grenvillian orogeny. Geology 39, 299–302.
Zhao, J.H., Zhou, M.F., Zheng, J.P., 2013a. Neoproterozoic high-K granites produced by melting of newly formed mafic-crust in the Huangling region, South China. Precambrian Research 233, 93–107.
Zhao, J.H., Zhou, M.F., Zheng, J.P., Griffin, W.L., 2013b. Neoproterozoic tonalite and trondhjemite in the Huangling complex, south china: crustal growth and reworking in a continental arc environment. American Journal of Science 313, 540–583.
Zhao, J.H., Zhou, M.F., Zheng, J.P., 2013c. Constraints from zircon U–Pb ages, O and Hf isotopic compositions on the origin of Neoproterozoic peraluminous granitoids from the Jiangnan Fold Belt, South China. Contributions to Mineralogy and Petrology 166, 1505–1519.
Zhao, X.F., Zhou, M.F., 2011. Fe–Cu deposits in the Kangdian region, SW China: a Proterozoic IOCG (iron-oxide-copper-gold) metallogenic province. Mineralium Deposita 46, 731–747.
Zhao, X.F., Zhou, M.F., Li, J.W., Sun, M., Gao, J.F., Sun, W.H., Yang, J.H., 2010. Late Paleoproterozoic to early Mesoproterozoic Dongchuan Group in Yunnan, SW China: implications for tectonic evolution of the Yangtze Block. Precambrian Research 182, 57–69.
Zhou, M.F., Kennedy, A.K., Sun, M., Malpas, J., Lesher, C.M., 2002a. Late Proterozoic arc-related mafic intrusions along the northern margin of South China: implications for the accretion of Rodinia. Journal of Geology 110, 611–618.
Zhou, M.F., Yan, D.P., Kennedy, A.K., Li, Y.Q., Ding, J., 2002b. SHRIMP zircon geochronological and geochemical evidence for Neoproterozoic arc-related magmatism along the western margin of the Yangtze Block, South China. Earth and Planetary Science Letters 196, 51–67.
Zhou, M.F., Ma, Y., Yan, D.-P., Xia, X., Zhao, J.H., Sun, M., 2006. The Yanbian Terrane (Southern Sichuan Province, SW China): a Neoproterozoic arc assemblage in the western margin of the Yangtze Block. Precambrian Research 144, 19–38.
Zhu, D., Luo, T.-Y., Song, X.-Y., Xu, Y.-G., Tao, Y., Huang, Z.-L., 2007. Advances in research on SORET effects in petrogenesis and metallogenesis of mafic-ultramafic rocks. Acta Mineralogica Sinica 27, 265–272 (in Chinese with English abstract).